CHALMERS

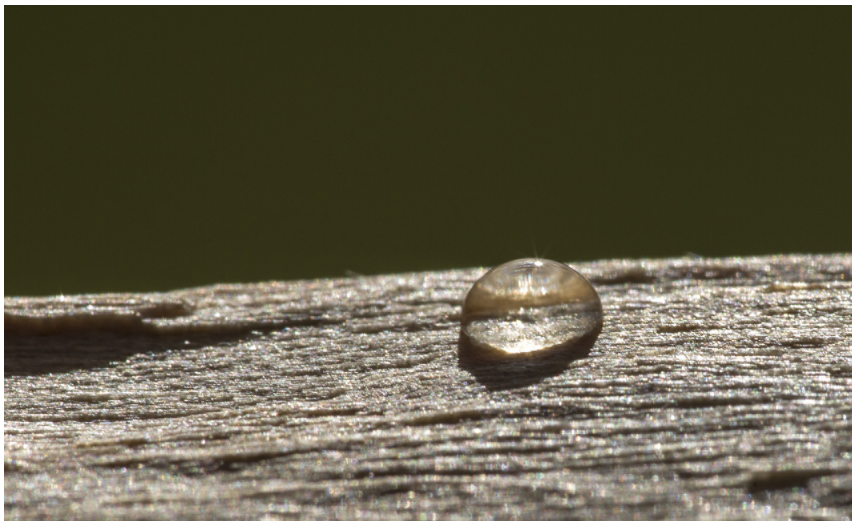

Separation of Droplets from Solids
- for drying of woodchips

Thesis for the Degree of Master of Science in Chemical Engineering

Erik Emanuel Andersson

Department of Chemical and Biological Engineering
Division of Chemical Engineering
Chalmers University of Technology
Göteborg, Sweden 2014

Thesis for the Degree of Master of Science

Separation of Droplets from Solids - for drying of woodchips

Erik Emanuel Andersson

Examiner:
Prof. Bengt Andersson
Supervisor:
Dr. Mohammad El-Alti

Department of Chemical and Biological Engineering
Division of Chemical Engineering
Chalmers University of Technology
Göteborg, Sweden 2014

Separation of Droplets from Solids
- for drying of woodchips

Erik Emanuel Andersson

Department of Chemical and Biological Engineering
Chalmers University of Technology
SE-412 96 Göteborg
Sweden
Telephone + 46 (0)31-772 1000

Cover: A water droplet placed on a woodchip surface.
Photograph by Tommy Andersson.

Printed by Chalmers Reproservice
Göteborg, Sweden 2014

Abstract

Woodchips is a solid biomass playing an important role for heat and power generation from renewable resources. The major quality factor for woodchips is the moisture content, wherefore drying is of greatest importance during production. This thesis is a study of a process separating liquid droplets from solid surfaces for drying of woodchips in a cyclone separator working at low temperature and pressure. Separation of phases instead of transfer between phases reduces the drying cost. In the process, the woodchips are first pressed in order to increase the surface area and to press water to the surfaces.

A theoretical understanding of the process is developed and the separation process of liquid droplets detaching from solid surfaces is simulated with the Volume of Fluid method. A trend study is performed in order to investigate the effects of varying wetting angle, droplet volume and relative velocity. It is shown that the detachment process is facilitated by a large contact angle, small droplet volume and high relative velocity. Also different orientations of the woodchip is investigated. The time frame for detachment is shown to be in order of milliseconds. For the process it is important to keep the time between press and cyclone as short as possible to get separation before the surface water is reabsorbed into the wood. In addition to the simulations, this thesis also includes an experimental part with observations and comments about the process.

Acknowledgements

This Master's thesis project has been performed at ALTEN Sverige AB and Chalmers University of Technology in Göteborg, Sweden, with the beginning in September 2013 and finalized in February 2014. The project has been supervised by Dr. Mohammad El-Alti from ALTEN Sverige AB and Professor Bengt Andersson and Assistant Professor Ronnie Andersson from Chalmers.

My greatest acknowledgments are directed to my supervisors Dr. Mohammad El-Alti, Professor Bengt Andersson and Assistant Professor Ronnie Andersson for their help and guidance throughout this thesis. I also want to address my thanks to the entire Analytics department and the Computational Fluid Dynamics group at ALTEN Sverige AB for the welcoming atmosphere. Thanks to group manager Elias Bernerskog, Niklas Persson and Erik Stendal for interesting discussions and their input and ideas throughout this thesis.

Last but not least I want to thank my friends, family and wonderful girlfriend for motivating and encouraging me to keep up the working spirit.

Nomenclature

Acronyms

CFD	Computational Fluid Dynamics
CFL	Courant-Friedrichs-Lewy number
CO	Carbon monoxide
CO_2	Carbon dioxide
$cwra$	Constant wetting rate angle
DNS	Direct Numerical Simulation
dpm	Discrete particle modeling
fsp	Fiber saturation point
HC	Hydrocarbon
LES	Large Eddy Simulation
MC	Moisture content
PAH	Polycyclic aromatic hydrocarbon
$RANS$	Reynolds Averaged Navier Stokes
RSM	Reynolds Stress Model
SST	Shear Stress Transport
$VLES$	Very Large Eddy Simulation
VOC	Volatile organic compound
VOF	Volume of Fluid

Greek symbols

α	Volume fraction
γ	Surface tension
ϵ	Dissipation of turbulent kinetic energy
θ_A	Advancing contact angle
θ_E	Contact angle
θ_R	Receding contact angle
μ	Dynamic viscosity
μ_t	Turbulent viscosity
ν	Kinematic viscosity
ρ	Density
ω	Specific dissipation rate

Roman symbols

E	Energy
F	Force
g	Gravitational acceleration
$\mathcal{H}$	Absolute humidity
k	Turbulent kinetic energy

L	Length
M	Molar mass
m	Mass
n	Amount of substance
P	Pressure
R	Length scale for droplet contour
r	Radius
S	Source term
T	Temperature
t	Time
u	Velocity
x	Space variable

Contents

1 Background and introduction

In this chapter, an introduction and background to this thesis is given in section 1.1. In section 1.2 the purpose of this thesis is presented and section 1.3 deals with the limitations that had to be set up.

1.1 Background

During the last centuries, increasing levels of carbon dioxide in the atmosphere have been recognized and a majority of all scientists are in agreement that human activities are contributing to those increasing levels. To impede the global warming following from the high CO_2 levels and stop the increase of natural disasters and extreme weather conditions something must be done [1]. In 2009 the European Union enacted a climate and energy package which includes a target of "Raising the share of EU energy consumption produced from renewable resources to 20 %" before year 2020 [2], in 2011 it was 13 % [3].

Apart from water-, wind- and solar energy, the most important renewable energy resource is biomass with the advantage of being controllable when and where to produce the energy. In order to fulfill the targets set by the EU mentioned above, a large number of biomass projects are planned for to complement the energy production from other renewable resources. Among the many types if biomass fuels, woodchips present good offers regarding availability and continuous supply. Historically, woodchips have been bought from local suppliers but with the increasing demand and with facilities projected in areas with low access to own supply, there will be a long distance between buyer and producer. It is thought that by 2020 the European Union will import about 30 % of the solid biofuel.

Fresh cut woodchips usually contain about 55 % water and by drying them, a lot is saved, both environmentally and economically, more specific in terms of lower transportation costs, increased heat economy and lower emissions during combustion. It has been shown that the drying procedure is the most costly part in the production process of woodchips and pellets. Therefore the idea of drying the woodchips in a mechanical way was born, more particularly to separate the moisture from the solid instead of the conventional approach with thermal drying, where moisture is removed by evaporation. In this way the energy consumption, and thereby the cost, can be significantly lowered since no heat is used to vaporize water. With a mobile drying unit, the drying can be performed at the place where the timber is harvested. The mechanical separation is to be done in a system consisting of a mechanical press and high speed air cyclone.

1.2 Purpose

The purpose of this thesis was to investigate and develop an understanding of the process separating liquid droplets from solid surfaces for drying of woodchips in a cyclone separator. In addition to the theoretical understanding, a model was built and CFD simulations of the separation of liquid droplets from a solid surface were performed. The simulation part includes a trend

study where wetting angle, droplet volume and relative air velocity have been varied in order to investigate how those changes affect the droplet detachment process. The simulations are made on a small scale considering an individual droplet placed on a single woodchip. The purpose of this thesis was never to perform full scale simulations of woodchips in a cyclone separator, but rather to build an understanding on a very small scale and to form a basis for future work.

In combination with the theoretical part, an experimental study has also been part of this thesis. This was done in order to obtain a deeper knowledge of the actual process and to make overall observations.

1.3 Limitations

As stated above, the simulations in this thesis focus on the separation of a single droplet from a solid surface. The trend study performed was done only for a two dimensional case. It was assumed that the gas stream always is flowing parallel to the woodchip. A 3D case was run for comparison with the 2D cases. No simulations of the actual process containing thousands of woodchips loaded into the cyclone were performed. Also, the evaporation of water was not included.

2 Theory

In this chapter the fundamentals about relevant topics are discussed. Section 2.1 explains woodchips in general with the focus on moisture content. In section 2.2 general drying mechanisms are discussed and section 2.3 describes how the drying process is set up. Section 2.4 gives a description of surface tension, wettability and sliding droplets while section 2.5 shortly describes the fundamentals about cyclone separators. Finally, section 2.6 covers the modeling procedure with governing equations and discrete phase modeling.

2.1 Woodchips

Woodchips are small pieces of wood, broken or cut from trees like the ones flaking off when felling a tree. They represent a very important solid fuel in facilities using biomass for generation of energy or heat. For the production of woodchips, large machines called wood-chippers are used and there are many different types of chippers where the largest ones can reduce entire trees to small woodchips. The dimensions of the produced chips are varying but typically in the range of 1-3 x 2-8 x 0-1 cm. In Figure 2.1 some examples of differently sized woodchips are to be seen.

Figure 2.1: Woodchips sorted by size.

2.1.1 Moisture content

Dealing with woodchips, the most important quality factor is the moisture content, MC, which can be calculated in two different ways; either on wet or dry basis. This means that the calculation is done by taking the ratio of moisture mass to the mass of either wet or dry material. In this

thesis all presented values of moisture content are given on wet basis, meaning that a sample of 1 kg woodchips with 50 % MC consists of 0.5 kg moisture and 0.5 kg dry wood. The MC (wet) is calculated according to Equation (2.1).

$$MC = \frac{m_{moisture}}{m_{dry\,wood} + m_{moisture}} \cdot 100\,[\%] \tag{2.1}$$

The moisture content in fresh cut wood is usually about 55 %, meaning that the majority of weight is water. The moisture in wood is present in different ways where the total amount is the free liquid water and the water vapor present in cell cavities and open spaces together with chemically bound water in the cell walls. The point when no water is present in the cavities and openings but the cell walls are saturated is called the fiber saturation point, fsp. The moisture content at this point can vary between different species and also between individual pieces of the same specie, but an average value of about 23 % MC is usually reported [4]. When drying wood with a moisture content above the fiber saturation point, i.e. for removal of free moisture, the mechanical and physical properties of the material remain unchanged, but drying below the fsp, the properties are functions of moisture content and thereby changed during the drying process. For pieces of wood with a MC below the fiber saturation point it is possible to determine an equilibrium moisture content at which the wood is neither loosing nor absorbing water and this equilibrium moisture content is highly dependent on relative humidity and air temperature.

As mentioned earlier, the moisture content is a measure of the quality of woodchips. A lot of moisture in the woodchips results in negative aspects when handling the chips, therefore it is desirable to reduce it. The reasons for aiming at a low moisture content is to

- avoid biodegradation of the material,
- decrease the transport costs,
- get higher efficiency during combustion,
- and to decrease the emissions during combustion.

In the following subsections, each point is described in more detail.

2.1.2 Biodegradation

Wood is a biodegradable material, meaning that enzymatic processes resulting from cell action can cause losses in performance or characteristics of the material [5]. The U.S. Geological Survey defines biodegradation as "Transformation of a substance into new compounds through biochemical reactions or the actions of microorganisms such as bacteria" [6]. The most important parameter affecting the degradation process is the moisture content. If the moisture content exceeds the fiber saturation point, about 23 %, the environment is favorable for growth of fungi and bacterias and therefore the degradation is very effective at high moisture content. If the moisture content is below 17 % no fungal decay can occur and the region in between those limits is a transition area in which decay might occur. If below 20 % MC no decay can be initiated [7].

2.1.3 Transport

Removal of moisture reduces the total material weight and thereby also the costs for transportation and handling. Consider two loads with woodchips having the same total weight, but the first has a MC of 50 % and the second is dried to 25 % MC. Comparing those shows that the

second contains 50 % more dry wood than the first. From this easy calculation it is clear that the costs for transport is reduced with lower MC; more wood can be transported to the same cost.

2.1.4 Energy content

Combustion of moisture-containing biomass fuels includes both the combustion itself, which is an exothermic reaction, but also the evaporation of water, which is an endothermic process. The energy required to evaporate the moisture must be taken from the burning fuel and thereby the amount of recovered energy is reduced. An increase in moisture content results in decreasing energy content per unit mass of fuel. The energy content is usually expressed as heating value and given as effective heating value of either dry or wet biomass. Shortly said, it is the amount of heat produced when a material is completely combusted. The moisture content is a factor strongly influencing the energy generated during the combustion process. The autothermal point is used to give the critical moisture content below which no additional fuel is needed after ignition, for biofuels this limit is about 65 %. In practice, combustors require the moisture content to be below 50 - 55 % [8]. For Scots pine, the relationship between effective heating value and moisture content is visualized in Figure 2.2, given on both dry and wet basis [9]. The more rapid decrease in heating value calculated on wet basis is due to the high increase in material weight with increased MC.

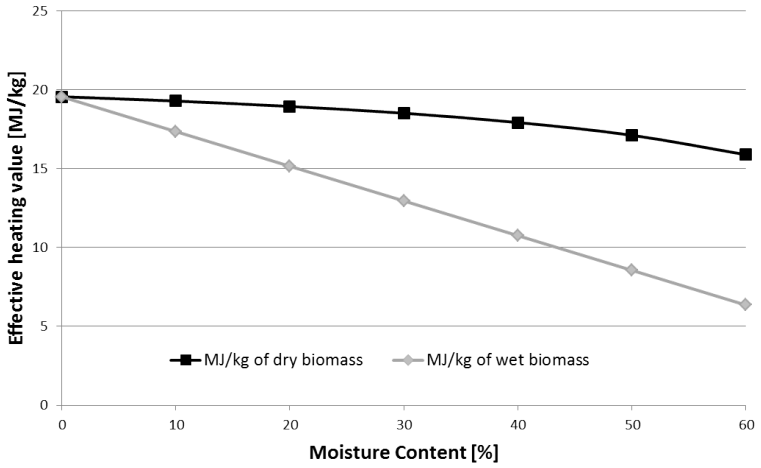

Figure 2.2: The effect of moisture content on the effective heating value of biomass from mature Scots pine stems, given on wet and dry basis respectively [9].

2.1.5 Emissions

During combustion of biomass, care must be taken of the pollutant emissions generated. A high moisture content results in a lower temperature in the combustion chamber, which might lead to incomplete combustion. This would increase the production of pollutant emissions of CO and HC, including volatile organic compounds, VOC, and polycyclic aromatic hydrocarbons, PAH, therefore the fuel moisture must be controlled properly [8].

2.2 Drying

The goal with drying is to remove the water saturated in the material. For wood this has historically been done by timber seasoning or piling up woodchips, where the former means that the timber is put at rest for a season before further handling. During this time of rest, the moisture content is decreasing due to evaporation, which is explained in section 2.2.1. Natural drying of wood over a summer reduces the moisture content to about 30 %.

2.2.1 Evaporation

Evaporation is the most well known way of drying and refers to transfer of water from a liquid to a vapor phase. For evaporation to take place, the vapor pressure of water must be higher than the partial pressure of moisture in the ambient gas. The partial pressure of water in air can be computed using absolute humidity, which is the ratio of water vapor mass to that of dry air, defined in Equation (2.2), where P_{tot} is the total pressure and M_{H_2O} and $M_{dry\,air}$ are the molar masses of water and dry air respectively. P_{H2O} is the partial pressure of water vapor defined in Equation (2.3) [10].

$$\mathcal{H} = \frac{M_{H_2O} P_{H_2O}}{M_{dry\,air}(P_{tot} - P_{H_2O})} \tag{2.2}$$

$$P_{H_2O} = \frac{n_{H_2O}}{n_{tot}} P_{tot} \tag{2.3}$$

In the above equation, n_{H_2O} and n_{tot} corresponds to the number of moles of water and the total number of moles respectively. Rewriting Equation (2.2) in terms of partial pressure of water vapor the following relation is obtained:

$$P_{H_2O} = \frac{\mathcal{H} M_{dry\,air}}{\mathcal{H} M_{dry\,air} + M_{H_2O}} P_{tot} \tag{2.4}$$

The amount of moisture in air is normally between 0.5 and 2 % [11] and combining this with the molar masses of air and water, 28.95 kg/kmol and 18 kg/kmol respectively [12] and an operating pressure of 1 bar gives a partial pressure of water of about 0.03 bar. Comparing this with the saturation pressure of water vapor at different temperatures shows that a temperature above 25°C is sufficient for evaporation to take place [13]. The temperature in the cyclone will be above this and therefore it is expected that water will also be evaporated inside the cyclone.

Observing the drying behavior of a wet solid material, it is possible to categorize the material in either of two groups. The first group includes granular and crystalline solids in which the moisture is held in pores between particles and the second group consists of amorphous, fibrous and gel-like solids in which the moisture is dissolved in fibers or very fine pores. The materials in the former group are mainly inorganic and unaffected by moisture removal, therefore the choice of drying method is not critical and the material can be dried fast. In the latter group, the materials are mainly organic, such as wood, glue and cotton. The effect of drying is often very high on those materials and therefore the drying process must be carried out very carefully to avoid too fast drying and thereby a damaged product. Within this scope of this thesis wood is to be dried and as just said, it belongs to the second group of materials. But kept in mind from section 2.1.1 is that drying above the fiber saturation point is not affecting the characteristics of the material. Moisture movement in solids of category two, as wood, above the fiber saturation point occurs by capillary action and below the fsp it is due to liquid diffusion.

For all solid materials, it is possible to observe a general behavior of the rate of change of moisture content during the drying process. Plotting the decrease in moisture content with respect to time gives the so called drying curve. Differentiating this curve with respect to time and multiplying with the ratio of solid dry mass to interfacial contact area, the drying rate flux as a function of moisture content is obtained. This function is plotted in Figure 2.3. The drying rate depends on temperature and moisture content of the solid material and on temperature, relative humidity and velocity of the ambient gas [10].

From Figure 2.3 it is clear that the drying process can be divided into different phases. From A to B is the preheating period where the material is heated to the drying temperature, some evaporation occurs with increasing rate. In Phase 1, from B to C, the surface is covered with water and the evaporation takes place with constant drying rate. During this period the rate-limiting step is the external mass and heat transfer. When the surface is no longer saturated with water, the critical point C is reached and the first falling rate period, Phase 2, is entered. In this period, the moisture must be transported from within the solid to the surface and the diffusional transport is controlled by internal liquid movement. Reaching point D, the material is still containing moisture and the drying continues until equilibrium is reached, for example at point E. Phase 3 is the second falling rate period, recognized for hygroscopic materials [10], [14].

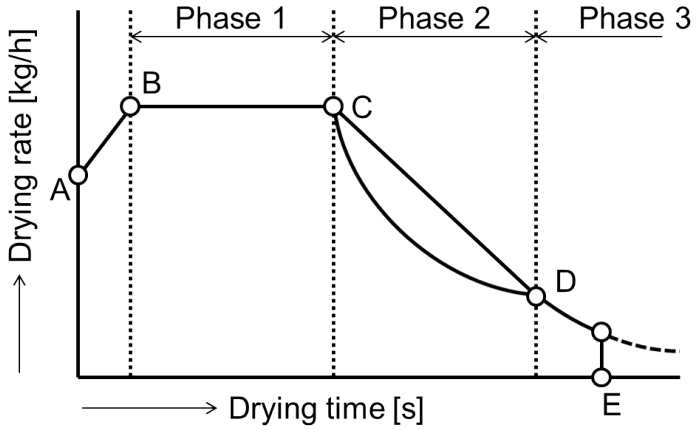

Figure 2.3: General drying rate curve, showing the different drying periods; The constant drying rate period, the first falling rate period and the second falling rate period.

2.3 Process

The main purpose of this thesis was to investigate the possibility of drying woodchips mechanically by separation of liquid droplets from the solid surface of woodchips. The process consists of a woodchipper, a mechanical press and finally a cyclone. In the woodchipper the chips are produced from stems of Scots pine and the fresh woodchips are then pressed in order not only to remove water directly but also to increase the surface area and the amount of surface moisture. The phase separation is then to be made in a high speed air cyclone where air is blown with high velocity around the woodchips. This generates a high relative velocity between the chips and the air. The fast traveling air phase will tear droplets off the wooden surface. More about the process in chapter 4.

2.4 Droplet physics

To develop some understanding of the physics of droplets, the following subsections, 2.4.1-2.4.3, are explaining surface tension, wettability and the behavior of droplets sliding on surfaces.

2.4.1 Surface tension

An important property of liquids is the surface tension, which can be understood by investigating the surface of a liquid, as the one depicted in Figure 2.4. Surface tension arises from the attraction between liquid molecules. In Figure 2.4 it is illustrated that a molecule within the liquid, completely surrounded by molecules of the same specie, experiences the same attraction in all directions, resulting in a zero net force. On the other hand, molecules at the surface, only have half as many neighbors of the same type and are therefore experiencing a net pull towards the liquid center. This is the reason why droplets are adapting their shape trying to minimize the surface area, and thereby also the surface energy. To move liquid molecules to the surface, and thereby increase it, work must be done. The measure of this work taken per unit area is the surface tension. In other words, the surface tension is the energy that must be supplied to increase the surface area by one unit [15].

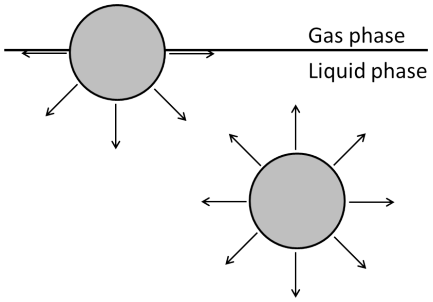

Figure 2.4: A surface molecule with half as many neighbors as the bulk molecules experiences a net inward pull.

Surface tension is dependent on both pressure and temperature but more strongly on the latter. In Equation (2.5) the surface tension for water in air is expressed as a linear function of temperature, where the temperature T is given in Kelvin [16]. With increased temperature the increased molecular motion overcomes the interactions and thereby the surface tension is reduced.

$$\gamma = 0.123(1 - 0.00139 \cdot T)\,[N/m] \tag{2.5}$$

2.4.2 Wettability

When a liquid is in contact with a solid surface, there will be interactions between molecules of the two phases. This phenomenon is called wetting and describes how a liquid behaves when deposited on a solid surface. There are different types of wetting, shown in Figure 2.5; total wetting with strong attractive forces to the surface, partial wetting with weaker forces and non wetting where the molecules are repelling each other. In the case with total wetting, droplets placed on the solid surface will spread completely forming a liquid film. On partially wetting surfaces, the droplets will remain in place forming a contact angle, θ_E, measured inside the droplet and used to characterize the surface. For contact angles approaching 180° the material

is said to be non-wettable. Between water and hydrophobic materials as paper and wood there are strong interactions compared to them between water and hydrophilic materials.

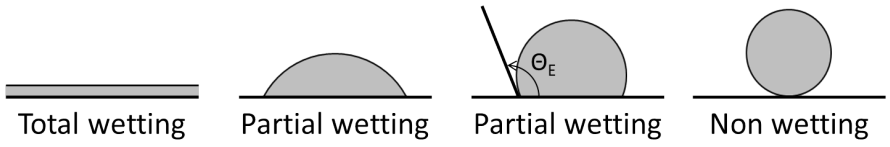

Figure 2.5: Wettability. Different degrees of wetting: total, partial and non wetting surfaces.

Nussbaum [17] studied how the wettability of wooden surfaces is reduced with time and made measurements of the constant wetting rate angle on different surfaces from two wood species. In Figure 2.6(a), a schematic graph for a droplet placed on a wooden surface is displayed. The upper part shows the contact angle against time after droplet application on the surface whilst the lower part displays the rate of change of contact angle. The wetting process can be divided into two major phases; first the contact angle is decreasing fast and the droplet is spreading on the surface, thereafter the rate of change of contact angle is leveling off and the contact angle becomes constant. This constant value is called the constant wetting rate angle, cwra, and in Figure 2.6(b) it is plotted against different times after the surface was cut. The presented graph is for water droplets placed on sawn tangential surfaces of Scots pine. It is seen that fresh and up to five days old woodchips have a cwra of about 40°. For older chips the cwra is increased, finally reaching about 70-80° for chips prepared more than 9 days in advance of the measurements. The reason behind increased cwra values on older surfaces is that wood extractives are transported to the surface, aiming at protecting the wood.

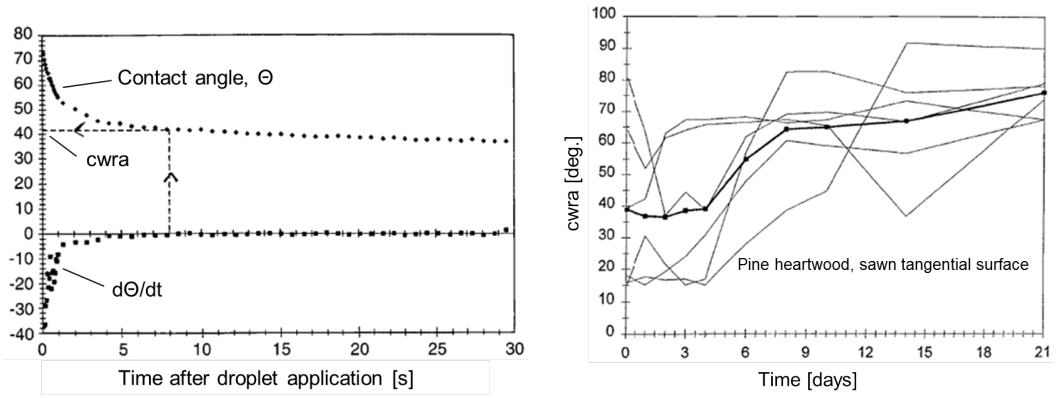

(a) (b)

Figure 2.6: Figure (a) shows that the contact angle initially decreases rapidly and then leveling off. In (b) the constant wetting rate angle, cwra, at different times after the cutting of new surfaces is displayed. Reprinted from Nussbaum [17] with clarified font.

A liquid droplet attached to a surface might change in volume, for example decrease due to evaporation or increase due to condensation of vapor from the ambient gas. Initially those two processes generate changes in contact angle while the contact area remains constant. This initial stage can be seen as a change in droplet height and continues until a critical contact angle

is reached, called the advancing or receding contact angle for increasing and shrinking volume respectively. When this critical contact angle is reached, it is kept constant and the droplet starts to change in diameter instead. The values of the advancing and receding contact angles are used to describe a material surface [18].

2.4.3 Sliding droplet

A droplet placed on a perfectly smooth horizontal surface will settle with a circular contact line and equal contact angle all around the circle. The contact angle, θ_E, for the droplet in thermodynamic equilibrium is described by the Young equation, Equation (2.6), relating the surface tensions between the solid and the vapor, the solid and the liquid, and the liquid and the vapor; γ_{SV}, γ_{SL} and γ, respectively [19].

$$\gamma_{SV} - \gamma_{SL} - \gamma \cos\theta_E = 0 \tag{2.6}$$

If an external force, as the aerodynamic force from a shear flow, is applied, the droplet will deform in the direction of the flow. In Figure 2.7, an example of the deformed droplet is displayed. The adhesion force is the force keeping the droplet in position, and is a function of the shape of the contact line and of the contact angle distribution. To describe of how the contact angle changes along the contact line, different models have been used in literature. For example Extrand and Kumagai [20] based their model on the advancing, θ_A, and the receding contact angle, θ_R, but experiments [21] have shown that the maximum and minimum angles, θ_{max} and θ_{min}, are not always equal to θ_A and θ_R.

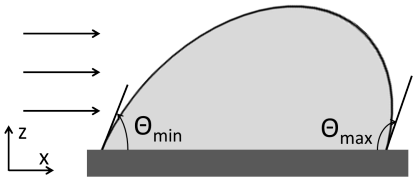

Figure 2.7: A droplet subjected to an external force is deformed and leaning in the direction of the external flow.

For droplet sliding to be initiated, both the maximum and the minimum contact angle must be attained, i.e. the contact angle is changing from θ_{min} to θ_{max} along the droplet perimeter. See Figure 2.7 for illustration of a sliding droplet with the angles illustrated. For known contact angle distribution along a known contact line, the adhesion force can be calculated with Equation (2.7). The difference in contact angle for a moving droplet is called hysteresis and is of importance in material science for design of surfaces with specific properties.

$$F_{adhesion,\,max} = \gamma\, R\, k(\cos\theta_{min} - \cos\theta_{max}) \tag{2.7}$$

In the above equation γ is the surface tension between the liquid and the gas, R is a length scale for the droplet contour and k is a parameter that must be determined by experiments. For known k the adhesion force can be predicted for a given combination of liquid/surface, but the disadvantage is that a new liquid or surface requires an experimentally determined update of k [22].

2.5 Cyclone separator

As described in section 2.3 the goal is to use a cyclone to dry woodchips by separation of water droplets from the wooden surfaces. In this section the basics of a cyclone separator are described.

A cyclone is a separation unit built upon the basic idea to separate solid particles from a gas stream, by use of the centrifugal force. In standard cyclones, the gas enters the device in tangential direction, bringing the gas into a swirly motion. The swirl is the tangential component of the flow velocity vector. The flow field shows the typical behavior of a combined vortex, where the gas flow is directed downwards in the outer region. Further down in the conical part the outer vortex is forced towards the center where the gas flows upwards in an inner vortex. The inner vortex is collected by the vortex finder and the gas exits the cyclone through the gas outlet on top. A typical reverse-flow cyclone is displayed in Figure 2.8, where also the inlet and outlets are named.

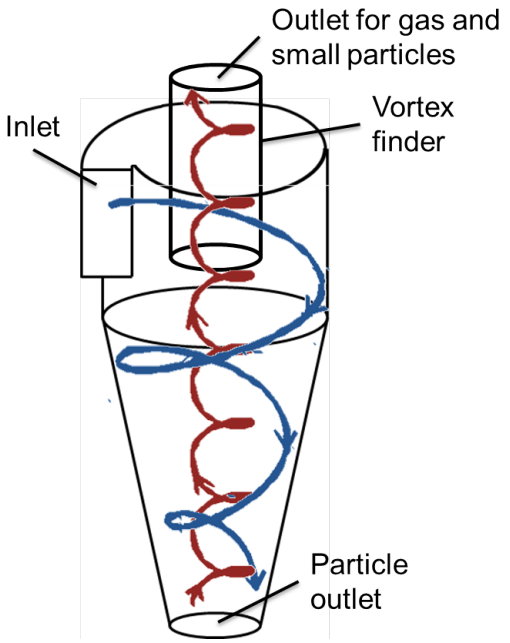

Figure 2.8: A reverse-flow cylinder-on-cone cyclone separator.

Particles enter the cyclone either together with the gas or through a separate inlet and the separation starts when they enter the swirly flow. Well inside, the particles are subjected to a strong outwardly directed centrifugal force bringing them towards the walls. The centrifugal force is highly dependent on the particle diameter and therefore larger particles will be easier to separate than small ones. At the walls, the particles will be brought downwards by the outer vortex, to some extent assisted by gravity. Apart from just separate solids from gas, cyclones can be used for classification of particles. In that case, lighter (smaller) particles will follow the gas stream out over top while larger particles will exit through the particle outlet at the bottom. Depending on cyclone dimensions and flow properties the break criterion can be determined [23, 24].

For a particle placed in the swirly flow, Newton's second law can be used to write the equation of motion:

$$(Mass \cdot Acceleration) = (Body\,force) + (Fluid\,drag) + (Unsteady\,force\,terms) \tag{2.8}$$

The body force is, for a particle falling in air, represented by the gravitational force and in a similar way, in a swirly flow, the particle will move relative to the gas and the gravitational force will be replaced by a centrifugal force pointing outwards in radial direction. The fluid drag is the drag force due to the relative velocity between the fluid and the particle and the unsteady force terms is a collection of all forces acting on the particle because of the particle acceleration relative to the fluid. All forces acting on particles in a multiphase flow are presented in Appendix B, where it also is stated which can be neglected.

The centrifugal force, $F_{centrifugal}$, is computed by Equation (2.9) where m is the particle mass, u is the particle's tangential velocity and r is the radius of the circular path.

$$F_{centrifugal} = m\frac{u^2}{r} \tag{2.9}$$

2.6 Modeling procedure

In this section, the modeling procedure is described, beginning with the governing equations and turbulence modeling, followed by multiphase modeling.

2.6.1 Governing equations

For fluid flows, the governing equations are the continuity equation for conservation of mass, (2.10), the equation of motion for momentum, (2.11), and an energy balance, (2.12). The equations are here given for a Newtonian fluid.

$$\frac{\partial \rho}{\partial t} + \frac{\partial \rho u_i}{\partial x_i} = 0 \tag{2.10}$$

$$\frac{\partial(\rho u_i)}{\partial t} + \frac{\partial(\rho u_i u_j)}{\partial x_j} = -\frac{\partial P}{\partial x_i} + \mu\frac{\partial}{\partial x_j}\left(\frac{\partial u_i}{\partial x_j} + \frac{\partial u_j}{\partial x_i}\right) + \rho g_i \tag{2.11}$$

$$\frac{\partial(\rho E)}{\partial t} + \frac{\partial(\rho E u_j)}{\partial x_j} = -\frac{\partial(P u_j)}{\partial x_j} + \frac{\partial}{\partial x_j}\left(k\frac{\partial T}{\partial x_j}\right) + \frac{\partial(u_i \tau_{ij})}{\partial x_j} + S_E \tag{2.12}$$

where S_E is an energy source term and the tensor τ_{ij} is defined as:

$$\tau_{ij} = \mu\left(\frac{\partial U_i}{\partial x_j} + \frac{\partial U_j}{\partial x_i}\right) - \mu\frac{2}{3}\frac{\partial U_k}{\partial x_k} \tag{2.13}$$

An equation of state, e.g. the ideal gas law, is used to relate pressure and internal energy to the state variables ρ and T and thereby the above equations can be solved [25].

In the ideal world, without limitations regarding computational power, time or money it would have been possible to solve those equations directly to give exact solutions perfectly describing the fluid behavior, but in general it is not possible to find an analytical solution because of nonlinearities and derivatives in both space and time, therefore a numerical solution method must be used.

The numerical solution is based upon dividing the computational domain into small cells and solve the governing equations numerically in each cell. A numerical solution brings an error, which should be as small as possible. By definition, the numerical error goes to zero as the cell size approaches zero, therefore a very fine grid is desired. But on the other hand a very fine grid requires much more computational power.

2.6.2 Turbulence modeling

Turbulence is characterized by fluctuating variables and for larger systems it is way too computationally expensive to achieve exact solutions to the governing equations. It is possible for smaller systems though, using DNS, which solves exactly in all computational cells. There are different ways of how much modeling is needed, for example by filtering in space like with LES or VLES. Another popular way to simplify the solution procedure and reduce the time for computation is to use the Reynolds decomposition, splitting the instantaneous variables, ϕ, into a time averaged part, $\overline{\phi}$, and a fluctuating part, ϕ', as shown in Equation (2.14). The averaged part is calculated whereas the fluctuating part is modeled.

$$\phi = \overline{\phi} + \phi' \tag{2.14}$$

Applying Equation (2.14) to all relevant variables and inserting into the conservation equations, (2.10)-(2.12), the so called Reynolds Averaged Navier Stokes, RANS, equations, are obtained. For convenience, when calculating compressible flows, a density weighted averaging procedure called Favre averaging is used in addition. An instantaneous variable is thereby decomposed as in Equation (2.15) where ϕ'' includes fluctuations of both turbulence and density. For incompressible flows with constant density ϕ'' equals ϕ'. The advantage with Favre- over Reynolds averaging is that the number of additional terms arising from density variations are reduced.

$$\phi = \widetilde{\phi} + \phi'' = \frac{\overline{\rho u}}{\overline{\rho}} + \phi'' \tag{2.15}$$

Favre averaging gives the following equations [25]:

$$\frac{\partial \overline{\rho}}{\partial t} + \frac{\partial (\overline{\rho} \widetilde{u_i})}{\partial x_i} = 0 \tag{2.16}$$

$$\frac{\partial (\overline{\rho} \widetilde{u_i})}{\partial t} + \frac{\partial (\overline{\rho} \widetilde{u_i} \widetilde{u_j})}{\partial x_j} = -\frac{\partial \overline{P}}{\partial x_i} + \frac{\partial}{\partial x_j} \left(\overline{\tau_{ij}} - \overline{\rho u_i'' u_j''} \right) \tag{2.17}$$

Writing the governing equations in terms of decomposed variables, unknown Reynolds stress terms are introduced, resulting in more unknowns than equations. There are different ways to handle this closure problem; either a transport equation for the Reynolds stress terms can be set up as in the RSM model, which in turn introduces new unknowns, or they can be modeled by introducing the Boussinesq approximation as done in the common two-equation models. In the latter case the components of the Reynolds stress tensor are modeled as proportional to the mean velocity gradients times an introduced turbulent viscosity, μ_t, analogous to molecular viscosity. The Boussinesq approximation is presented in Equation (2.18) where $k = \frac{1}{2}(\overline{u_i' u_i'})$ [25].

$$\tau_{ij} = -\rho \overline{u_i u_j} = \mu_T \left(\frac{\partial \overline{u_i}}{\partial x_j} + \frac{\partial \overline{u_j}}{\partial x_i} \right) - \frac{2}{3} \rho k \delta_{ij} \tag{2.18}$$

Comparison between the RSM model and the two-equation models reveals that the latter assumes isotropic turbulent viscosity, thereby, even though the RSM model introduces new unknowns they are of higher order which generates a more accurate solution. On the other hand, with increased number of transport equations to be solved, the RSM model is much more computationally heavy [27].

For practical problems it has been shown that the turbulence model should include, at least, two equations to give successful results. Solving for two quantities, the turbulent length and velocity scales can be determined independently. The popular two equation models include, as one of the two equations, the transport equation for turbulent kinetic energy, k, presented in Equation (2.19) for incompressible flows.

$$\underbrace{\frac{\partial k}{\partial t}}_{\text{(I)}} + \underbrace{\overline{u_j}\frac{\partial k}{\partial x_j}}_{\text{(II)}} = \underbrace{-\overline{u_i' u_j'}\frac{\partial \overline{u_i}}{\partial x_j}}_{\text{(III)}} \underbrace{-\nu\left(\overline{\frac{\partial u_i}{\partial x_j}\frac{\partial u_i}{\partial x_j}}\right)}_{\text{(IV)}} + \frac{\partial}{\partial x_j}\left(\underbrace{\nu\frac{\partial k}{\partial x_j}}_{\text{(V)}} - \underbrace{\frac{\overline{u_i u_i u_j}}{2}}_{\text{(VI)}} - \underbrace{\frac{\overline{u_j p}}{\rho}}_{\text{(VII)}}\right) \tag{2.19}$$

(I). Accumulation of turbulent kinetic energy, k.

(II). Convection of k by the mean velocity.

(III). Production of k; energy is extracted to the large eddies from the mean flow.

(IV). Dissipation of k by viscous stress; turbulent kinetic energy is transformed into heat.

(V). Molecular diffusion of k.

(VI). Transport of k by velocity fluctuations.

(VII). Transport of k by pressure fluctuations.

In the above equation, closures are needed for the terms (III), (IV), (VI) and (VII). As mentioned before, the Boussinesq approximation, Equation (2.18), is used to model the unknown part of term (III). Term (IV) is defined as the dissipation of turbulent kinetic energy, ϵ, and solved by setting up a transport equation for ϵ individually. To describe the turbulent transport, terms (VI) and (VII), a gradient-diffusion transport mechanism is assumed. [27]

One of the most used turbulence models is the standard $k-\epsilon$ model which solves one transport equation for k and one for ϵ. This model is well suited for flows where the turbulence is almost isotropic. Therefore it cannot be used close to walls and there is a need to implement wall functions.

Another widely used two equation model is the $k-\omega$ model, including one transport equation for k and one for the specific dissipation rate, ω, which can be seen as the turbulence frequency. ω is the quantity used for determination of the length scale and is proportional to ϵ/k. When using the $k-\omega$ model no wall functions are necessary since the model has been proven to predict the law-of-the-wall in an appropriate way.

The following transport equation is used for modeling of ω in incompressible flows:

$$\frac{\partial \omega}{\partial t} + \overline{u_j}\frac{\partial \omega}{\partial x_j} = \alpha\frac{\omega}{k}\nu_T\left[\left(\frac{\partial \overline{u_i}}{\partial x_j} + \frac{\partial \overline{u_j}}{\partial x_i}\right)\frac{\partial \overline{u_i}}{\partial x_j}\right] - \beta^*\omega^2 + \frac{\partial}{\partial x_j}\left[\left(\nu + \frac{\nu_T}{\sigma_\omega}\right)\frac{\partial \omega}{\partial x_j}\right] \tag{2.20}$$

Finally closing the $k-\omega$ model, the turbulent viscosity is calculated with $\nu_T = k/\omega$ and the closure coefficients appearing in the model are assumed constant.

The Shear-Stress Transport (SST) $k-\omega$ model is combining the standard $k-\epsilon$ model with the $k-\omega$ model by using a blending function, which generates a gradual transition between the two models. This model utilizes that the standard $k-\epsilon$ model is proven to perform well where the flow is fully turbulent and that the $k-\omega$ is well predicting the flow close to the walls. A modified formulation of the turbulent viscosity is used to account for the transport effects of the principal turbulent shear stress [26].

2.6.3 Discrete phase and VOF

When the single phase problem with a gas phase flowing around a woodchip is solved, the subject was to introduce droplets on the surface and thereby the problem became multiphase. In this thesis the Volume of Fluid, VOF, method has been used as multiphase model. The VOF model is a technique tracking the interface between two, or more, immiscible fluids, by solving only a single set of momentum equations and turbulence model shared between the phases. The multiphase problem is thereby treated as quasi-single phase but with variable properties depending on the volume fractions of all phases. The phases are not allowed to be interpenetrating.

In each computational cell, the volume fraction of phase i, α_i, can take all values from zero to one; $\alpha_i = 0$ means that the cell contains nothing of phase i, $\alpha_i = 1$ indicates that the cell is completely filled with fluid i. When $0 < \alpha_i < 1$, more than one fluid is present and the cell must contain the interface between the phases. For such cells, variables and properties are represented as mixtures depending on the volume fraction values. For example, the density in a cell with n phases is calculated with Equation (2.21). In this way sudden changes in fluid properties when passing an interface are avoided [26].

$$\rho = \sum_{i=1}^{n} \alpha_i \rho_i \tag{2.21}$$

The actual interface tracking is made with a continuity equation, (2.22), for the volume fraction of one, or more, of the phases.

$$\frac{1}{\rho_q}\left[\frac{\partial}{\partial t}(\alpha_q\rho_q) + \nabla\cdot(\alpha_q\rho_q\vec{v}_q) = S_{\alpha_q} + \sum_{p=1}^{n}(\dot{m}_{pq} - \dot{m}_{qp})\right] \tag{2.22}$$

where $\dot{m}_{pq}$ is the mass transfer from phase q to phase p and $\dot{m}_{qp}$ the opposite. Because no cell can contain a volume fraction greater than unity, the volume fraction of the primary phase is calculated with:

$$\sum_{i=1}^{n} \alpha_i = 1 \tag{2.23}$$

Specific values of the volume fraction does not correspond to a certain shape of the interface, rather many different shapes in each computational cell are possible. Therefore a geometric reconstruction scheme must be used. By knowing the volume fraction of each phase in the neighboring cells a reconstruction of the interface is done.

Modeling of the surface tension has in this thesis been made with the Continuum Surface Force model in the way that a source term is added to the momentum equation. In Fluent, local gradients of the surface normal are used to get the surface curvature and then the surface tension is written in terms of the jump in pressure over the interface. The force at the surface is expressed as a volume force, which is the source term included in the momentum equation. Surface tension effects are more accurately calculated on hexahedral and quadrilateral meshes than on tetrahedral and triangular meshes [26].

3 Method

This chapter gives a description of the methods used during the simulations as well as of the preparations made in advance. First, the two-dimensional case is presented in section 3.1 and thereafter the 3D case is treated in section 3.2.

In all computer simulations, one single woodchip was studied and in the 2D cases a single droplet was placed on the woodchip surface. In the 3D simulation, three droplets were patched onto the surface. All geometries were constructed and meshed in the software ANSA 14.1.0 and the CFD simulations were performed in ANSYS Fluent 14.5. In the simulations in this thesis a chip of size of 6.0 x 1.5 x 0.5 cm has been used. The reason for choosing such a long chip was to be able to see the droplet sliding on the surface. In 2D the dimensions 6.0 x 0.5 cm have been used.

3.1 2D simulations

The purpose of this thesis was modeling the separation process when liquid droplets separate from a solid surface. First a 2D simulation was made and by solving only in two dimensions the computational time needed was clearly reduced compared to perform 3D simulations. First, the geometry and mesh are described in subsection 3.1.1, followed by the simulation details, boundary conditions and convergence in subsections 3.1.2, 3.1.3 and 3.1.4 respectively. Thereafter the discrete phase implementation, dynamic mesh adaption and time step size are treated in subsections 3.1.5, 3.1.6 and 3.1.7. Finally, in subsections 3.1.8 and 3.1.9, the trend study and the different orientations of the woodchip are discussed.

3.1.1 Geometry and mesh

A 2D geometry of a single woodchip placed in a windtunnel was constructed and a schematic view of the computational domain is displayed in Figure 3.1. Note that only a single woodchip is under consideration. The dimensions of the woodchip selected for the simulations was 60 x 5 mm, which is to be seen as a large woodchip used in the system. Other dimensions used in the simulations are the height and length of the windtunnel, chosen large enough to get a fully developed airflow upstream the woodchip and not to have the walls affecting the flow around it. Chosen dimensions were a height "h" of 1200 mm and a length "L" of 2400 mm, which correspond to 20 x 40 woodchip lengths. In Figure 3.1 also the inlet and outlet are shown.

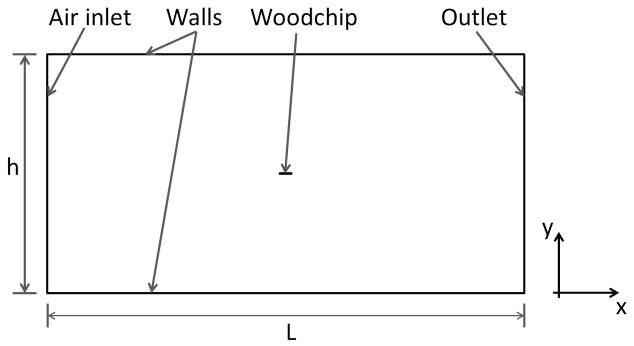

Figure 3.1: Schematic of the computational domain used for 2D simulations.

A structured mesh with only quadrilateral elements was generated with high resolution closest to the woodchip and gradually decreasing further away. A close up around the woodchip is displayed in Figure 3.2. The number of cells in the full 2D mesh was in the order of 110 000. To control the cell size and growth rate, the spacing between different cell nodes was defined. The quality of the mesh was evaluated considering aspect ratio and skewness.

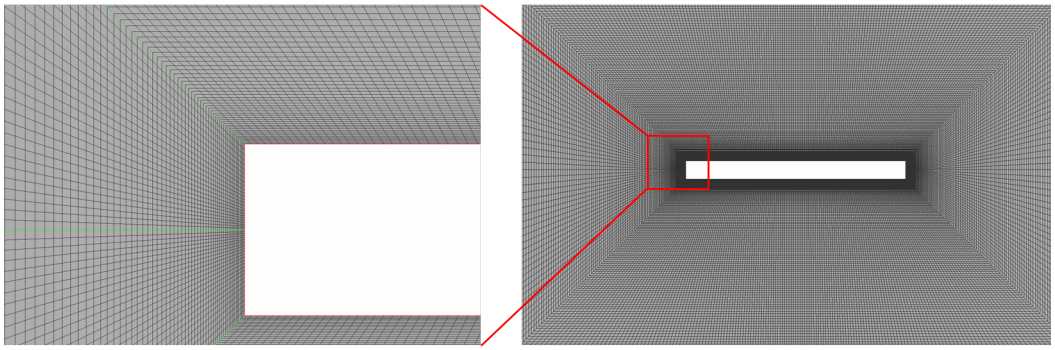

Figure 3.2: The two dimensional computational mesh shown in a close up around the woodchip.

3.1.2 Simulation settings

The single phase flow field simulations were solved steady-state with the pressure-based coupled solver. Compared to segregated solvers, this coupled algorithm shows better performance with a robust and efficient implementation for single phase steady flows. By solving the momentum and continuity equations together a faster convergence is obtained [26].

Modeling turbulence, the SST $k-\omega$ model was used, a good model with respect to accuracy and computational cost. It was chosen because it has been proven to perform well both close to the walls and in the fully turbulent bulk flow. The steady-state flow was solved with the pseudo transient under-relaxation method. This enables an implicit under-relaxation control of the equations via a pseudo time step size [26]. Initially a first order upwind discretization scheme was used, eventually changed to a second order scheme in order to obtain a more accurate solution and remove any numerical diffusion [27]. For pressure the PRESTO!-scheme was used.

3.1.3 Boundary conditions

First a single phase simulation was made to solve the gas flow field around the woodchip. The boundary conditions used for the inlet and outlet were set as velocity inlet and pressure outlet respectively. At the inlet a turbulent intensity of 5 % and length scale of 0.35 mm (7 % of woodchip height) were defined [27]. Different inlet velocities were applied for different cases. The operating conditions were set to 60° C and atmospheric pressure. Both the tunnel walls and the woodchip surfaces were defined as walls and for the tunnel walls a zero shear boundary condition was set while a no-slip condition was used for the woodchip surfaces.

3.1.4 Convergence

Judging whether a solution has converged or not, the scaled residuals for momentum, continuity, turbulence and velocities were first considered. They should continuously be below a specified value, e.g. 1e-04 or 1e-06. Additional criteria must also be monitored since low residuals do not automatically rule out an incorrect solution. On the other hand, a solution might be valid also with higher residuals. In this thesis, area weighted average of velocity and of turbulent kinetic energy were monitored over planes in the geometry. Those averages should be constant for the solution to be considered converged. Also the mass imbalance should be considered, not to loose or gain mass inside the system.

3.1.5 Discrete phase

With a second phase, several additional settings have to be defined. In this thesis the multiphase model Volume of Fluid, VOF, has been used. The different phases must be specified and if the initial volume fraction of one of the phases is to be patched into an area of the domain, that phase should, for convenience, be the secondary phase [28]. Therefore, air was chosen as primary phase and liquid water as secondary. The physical properties of the air was set for a temperature of 60°C and for water of 15°C. For the interaction between the phases, the surface tension was, according to Equation (2.5) for 60°C, specified to 0.066 N/m. Also the option wall adhesion was enabled, thereby the contact angle between the water droplet and the wall could be defined. This value is used to adjust the surface normal in the cells near the walls. The adhesion angle is implemented as a boundary conditions at the different walls. At the tunnel walls an angle of 175° was used to define the surface as non-wettable and at the woodchip surfaces the contact angle was defined according to the different values for the different cases run. In the boundary conditions tab it should be defined that the volume fraction of water at the inlet is zero, i.e. only air is entering. The same holds for the backflow at the outlet. The case was solved transient with an explicit scheme. For the volume fraction, the geometric reconstruct scheme was used.

The imposition of a droplet was made the way described in Figure 3.3 by first using the function "Adapt - Region" to mark in which cells the water droplet should be placed initially. Thereafter the function "Patch" under the "Solution Initialization" tab was used to define that the marked region, i.e. the droplet, only should contain water. To start the calculations with a smooth droplet surface the procedure was repeated some times.

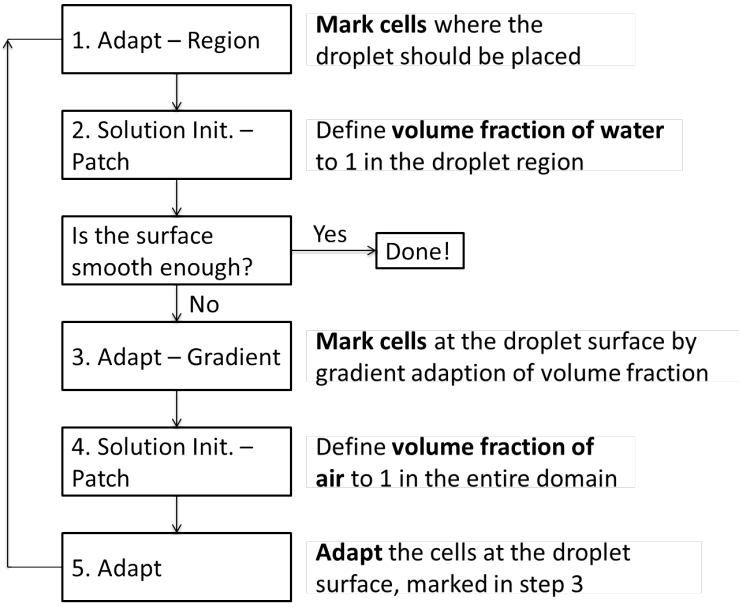

Figure 3.3: Iterative procedure for introducing a smooth droplet.

3.1.6 Dynamic mesh adaption

When performing VOF simulations it is desired to have very small cells in the region of the phase interface, to be able to resolve it as good as possible. In addition to this, the fact that the droplets are moving requires a very fine mesh over a large area. Instead of initially using a very fine grid over an unnecessarily large area, a dynamic mesh adaption method has been used in this thesis. This locally changes the mesh at given intervals and with respect to given properties. In this thesis the refinement was done with respect to gradient of volume fraction of water. It is also possible to coarsen the mesh but in this project this feature was turned off since the total number of cells was still considered low and if merging cells (=coarsening), information already calculated for all nodes at the fine mesh get lost. The area where coarsening was possible was upstream the droplet and coarsening would therefore have affected the flow field in the droplet area.

3.1.7 Time step

Determining the time step size, the Courant number, CFL, was used. The CFL number is defined according to Equation (3.1) where u is the flow velocity, Δt is the time step size and Δx is the cell size in the flow direction.

$$CFL = \frac{u \cdot \Delta t}{\Delta x} \tag{3.1}$$

A general rule is that the time step used should be less than the time it takes for transport through one computational cell. Thereby it should be chosen according to:

$$\Delta t < \frac{CFL \cdot \Delta x}{u} \tag{3.2}$$

For calculations with an explicit solver it is desired to have CFL<1 and when using an implicit solver CFL should be about 5. In the latter case it is important that the solution is stable in all time steps and therefore it is recommended to start with a small Courant number and gradually increase it at later time steps [27].

3.1.8 Trend study

In the cyclone there will be different parameters affecting the separation process where droplets detach from the solid surface. Three parameters were identified as relevant to investigate and a trend study has been performed. The parameters investigated are presented in Table 3.1, where also the lower and upper levels for each parameter are shown. Note that the gas flow velocity is normalized with respect to the upper level.

Table 3.1: Parameters and levels used in the trend study.

Parameter	Lower level (-)	Upper level (+)
Contact angle, θ	20°	80°
Droplet volume, V	0.5 μl	30 μl
Gas flow velocity, u	0.42	1

The levels for each parameter were determined in the following way:

In the press, new faces are produced and thereafter the contact angle follows the behavior of Figure 2.6(a), ending up at values between 20 and 80° for fresh chips, as seen in Figure 2.6(b). Therefore the **contact angle** was assumed to vary between 20 and 80°.

The **droplet volume** was assumed to vary between 0.5 and 30 μl which corresponds to spheres with a diameter between 1 and 4 mm, which is about the size of raindrops [29].

The **relative velocity** was extracted from a previous simulation study on a similar cyclone by inserting the woodchip properties and comparing the particle velocity with the velocity of the gas flow. The normalized relative velocity was determined to vary between about 0.42 and 1 [30].

A full factorial design was used to set up which simulations to perform. With three parameters at two levels each this resulted in $2^3 = 8$ simulations. The design matrix is presented in Table 3.2.

Table 3.2: Design matrix for full factorial design with three parameters, each at two levels.

Design Matrix				
		θ (a)	V (b)	u (c)
1	(1)	-	-	-
2	(a)	+	-	-
3	(b)	-	+	-
4	(ab)	+	+	-
5	(c)	-	-	+
6	(ac)	+	-	+
7	(bc)	-	+	+
8	(abc)	+	+	+

3.1.9 Orientation

The woodchips in the cyclone will be oriented in different ways and the droplets will be present on all sides. The result of this is that the centrifugal acceleration, due to the rotational motion, is either assisting or opposing the phase separation process. To investigate the effect of a differently directed centrifugal acceleration, five different cases were simulated. In Figures 3.4 the different directions used in the simulations are shown. In Fluent the centrifugal acceleration was implemented as gravity. In those simulations the parameters considered from the trend study were fixed to a contact angle of 40°, a droplet volume of 15 μl and a normalized relative velocity of 0.75.

(a) Directed upward. (b) Directed downward.

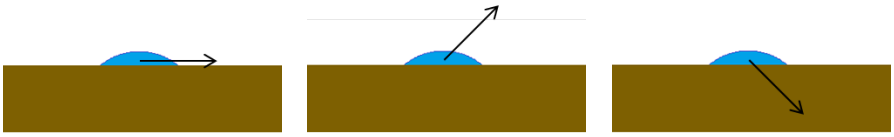

(c) Directed to the right. (d) Directed up and right. (e) Directed down and right.

Figure 3.4: The five cases representing different orientations of the woodchip. The arrows are indicating the direction of the centrifugal acceleration.

3.2 3D

For the three-dimensional simulation, a hybrid mesh was generated. To maintain the fine resolution close to the woodchip this area was extruded in the third dimension by defining a distance and how many layers to be used, resulting in a structured hexahedral mesh. Further away from the chip, a triangular surface mesh was generated and thereafter this outer volume was meshed with the tetra rapid algorithm, which is a fast method generating tetrahedral elements. The 3D case represents a 15 mm wide woodchip. A cross section of the mesh is to be seen in Figure 3.5.

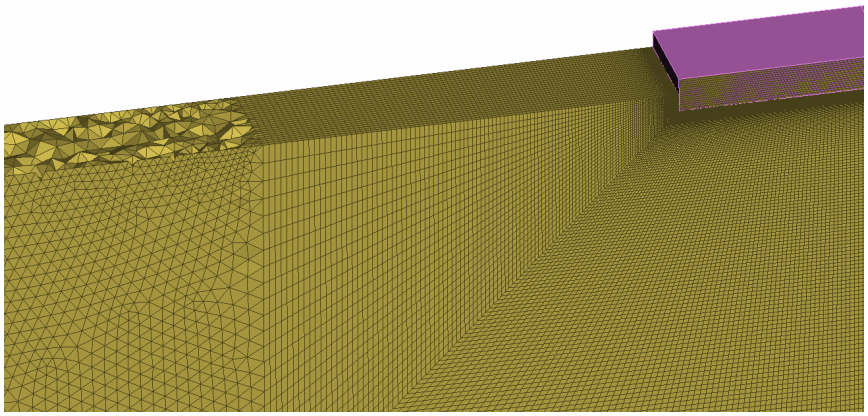

Figure 3.5: Cross section of the 3D computational mesh. Closest to the chip, structured hexahedral elements are used, while tetrahedral elements are used further away.

The procedure for setting up the 3D case was basically the same as in the the 2D case described above. Due to convergence problem using a compressible solver, the flow field around the woodchip was solved incompressible, steady-state with the pressure-based coupled solver. In the 3D case, three droplets were patched onto the woodchip surface, as is visualized in Figure 3.6 where the woodchip with applied droplets is seen from above.

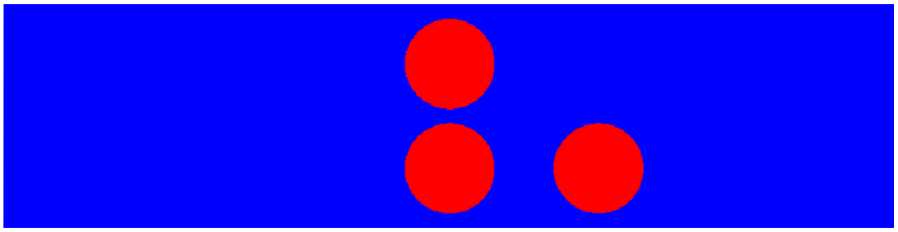

Figure 3.6: Woodchip seen from above with three droplets patched onto the surface. Woodchip colored in blue, droplets in red.

In 3D, one case was run, with a contact angle of 40°, a droplet volume of 15 μl and a normalized relative velocity of 0.75, the same parameter values as in the simulations with different orientation. In this 3D case the centrifugal acceleration was directed as in Figure 3.4(d).

4 Experimental study

Within the scope of this thesis, pilot scale experiments have been performed in order to develop a deeper understanding of the process as a whole and to get ideas of which parameters that are feasible to change for optimization purposes. In this chapter, the process is first described in combination with observations and experimental results. Thereafter, the main results and conclusions from a separate experimental study [31] of the woodchip drying process in a cyclone are presented.

4.1 Experimental setup

The performed experiments were the first ones on a completely new pilot unit, therefore the main purpose was process understanding and overall observations, not to focus on detailed results.

Fresh cut woodchips, with a moisture content of 60 % were taken from a woodchipper and driven through a mechanical press, where they were significantly deformed and a lot of moisture was pressed out to the woodchip surfaces. Just by hand it was possible to feel a clear difference in the amount of surface water after, compared to before, the press. It was seen that most of the water was pressed out on the short sides of the woodchips, where the fibers were cut. By inspection it was not possible to determine whether there were droplets or a water film on the surface. Leaving the pressed chips at rest for some time showed that the water was reabsorbed into the interior of the chips, in accordance with the theory. Measuring the moisture content in those chips, where the water was reabsorbed, only a small difference from the fresh ones was observed. A conceptual description of the mechanical press is to be seen is Figure 4.1(a).

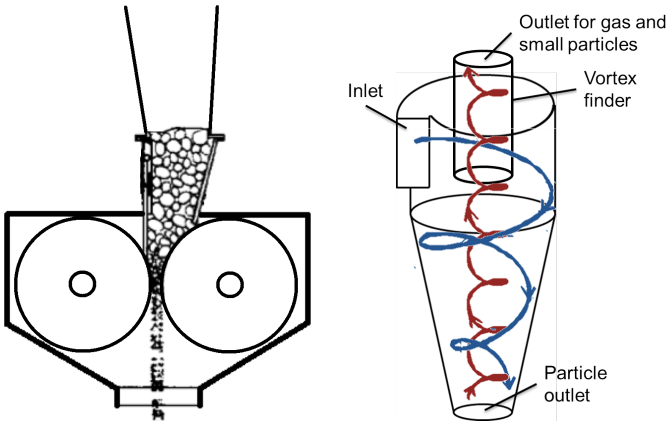

Figure 4.1: Conceptual figures of the mechanical press (a) and the high speed air cyclone (b) used in the experiments.

The pressed woodchips were further transported on a conveyor to the cyclone. According to Figure 2.6(a) the time between press and cyclone should be as short as possible, in order to have as large contact angle as possible, therefore it would be beneficial to remove the conveyor belt and place the cyclone inlet just at the press.

In the cyclone, the residence time was observed to vary quite a lot, between just a few up to more seconds, depending on particle size and loading. It was noted that smaller chips had a shorter residence time than larger chips. A higher loading of woodchips also generated a shorter residence time. Focus was not on the actual measured residence times but on the fact that they were varying. There was a notable difference in how wet the chips appeared before and after the cyclone. Measurements showed that the moisture content was reduced to about 50 %. It was seen that the smallest particles left the cyclone together with the air stream over head. Those particles were all dry. Since this was the first experiments performed, neither the press nor the cyclone were optimized and the operating conditions, e.g. the air speed, were much below desired levels. A conceptual description of the cyclone used in the experiments is shown in Figure 4.1(b).

Even though a lot of moisture was pressed out of the wood in the press it was not possible, with the present equipment, to separate any of it between press and cyclone. This might be solved by introducing a conveyor belt with some kind of vacuum suction. In that way some of the separated water is removed before the cyclone.

A series of designed experiments have been carried out on a cyclone [31]. Apart from a slightly smaller cyclone diameter, the process was the same as in the above described experiment. Together with a subsequent data analysis the effects of geometry and process variables on the drying process were investigated. The considered process responses were; average moisture content after the cyclone [%], mass of removed moisture [kg/h] and blower energy use per mass of removed moisture [kWh/kg]. Multivariate data analysis, MVDA, was used to identify the most dominant parameters behind the different responses. The experiments showed that in order to achieve a low average MC in the product, the feed rate should be low and the blower speed should be high. To remove as much moisture per time [kg/h] as possible, it was shown that a high feed rate and high blower speed were most beneficial. It was seen that a low feed rate resulted in longer residence time which in turn resulted in a drier product. In contrast, a high feed rate resulted in more moisture removed per time but the product then had a higher moisture content. The feed rate was the most influencing parameter regarding both average MC after and removed moisture per time. Also for the blower energy use per removed moisture, the feed rate was shown to be the most influencing parameter in the way that a high feed rate means low energy use per kg removed moisture and vice versa. A low feed rate gave drier product but with reduced energy efficiency. The lowest energy use per kg removed moisture was achieved with high feed rate and low blower speed. It was also proven that removal of the first percentages of moisture required least blower energy.

5 Results

This chapter presents the results from the calculations and simulations made. First, the results from the single phase problem with a gas flowing around a woodchip are presented in section 5.1, followed by section 5.2 where the boundary layer is investigated. Thereafter the problem was made multiphase by inclusion of water droplets on the surface and the results from those simulations with different values of the parameters are presented in section 5.3. In section 5.4 the results from the simulations with differently directed centrifugal acceleration are presented. This is followed by section 5.5, with results from hand calculations of a liquid film placed on the woodchip surface.

5.1 Flow field, two-dimensional

In Figure 5.1 the two dimensional single phase flow field is displayed. The figure is a close up around the woodchip and it can be seen that there is a stagnation point at the woodchip surface where the gas flow hits the solid body and thereby the velocity is brought to zero. Behind the woodchip, a region of recirculation, a wake, can be seen as the blue region. Along the top and bottom surfaces it can be seen that the flow is accelerating. The areas of low velocity above and under the chip are described more in the following section. The normalized free stream velocity is 0.75.

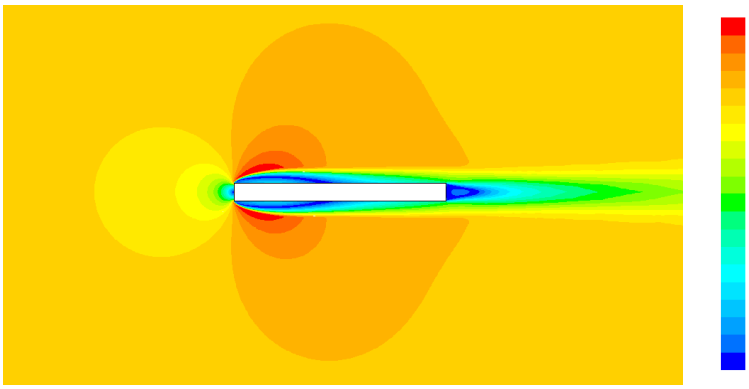

Figure 5.1: Close up of the 2D gas phase flow field around a single woodchip. The figure is colored by normalized velocity magnitude, ranging from 0 to 0.97. The normalized free flowing gas velocity is 0.75.

5.2 Boundary layer

In section 3.1.3 it was stated that the no-slip condition was used as a boundary condition at the woodchip surfaces. This means that the relative velocity between the solid and the fluid is zero

and thereby the first layer of fluid molecules are not moving at all in the flow direction, only bouncing back into the fluid, slowing down the fluid flow. Because of this, a gradual change in flow velocity is observed, this is the so called boundary layer. The boundary layer thickness is taken as the point where the flow velocity is 99% of the free stream velocity [16].

In Figure 5.2 the x-velocity profiles at four different locations along the woodchip surface are plotted as functions of distance above the surface. In addition, a red line indicating 99 % of the free stream velocity is included. The points of intersection between the velocity profiles and the red line is the boundary layer thickness at the four different positions. It can be seen that it is about 4 mm thick everywhere, thereby it can be concluded that the water phase will be entirely located in the boundary layer. The largest drops in this thesis had a height of 2.2 mm.

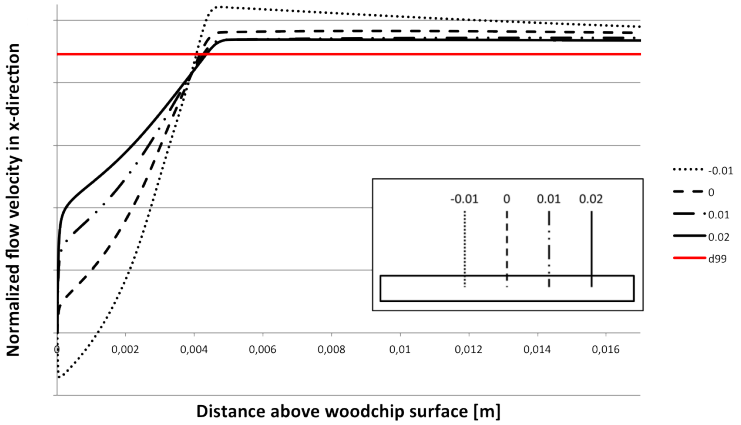

Figure 5.2: Normalized velocities in x-direction at different locations against distance above the surface. The normalized velocity ranges from -0.17 to 0.83. The inset shows where on the woodchip the different velocity profiles are measured. "d99" represents 99% of the free stream velocity.

5.3 Trend study

One purpose with this thesis was to perform a trend study to investigate how different parameters are influencing the separation process. As described in section 3.1.8 above, a full factorial design was used to plan which simulations to perform. The eight simulations presented in Table 3.2 were run to see the effects of droplet size, contact angle and flow velocity. The results are presented in subsections 5.3.1, 5.3.2 and 5.3.3 respectively. In all simulations the droplet was placed on the middle of the chip.

5.3.1 Contact angle

In Table 3.2 it can be seen that there are pairs of simulations having exactly the same settings but for one parameter. Beginning with the contact angle, it is seen that the simulations 1-2, 3-4, 5-6 and 7-8 form four pairs in which only the contact angle is different. Therefore the effect of a changed contact angle can be evaluated by comparing those pairs individually.

In Figure 5.3 the droplet locations after 1.2 ms in simulations 1 and 2 are presented. In the first case the surface is more wettable than in the second, resulting in a stronger bond between the droplet and the surface. In the figures, this phenomenon can be seen in the way that the droplet in Figure 5.3(b) is detached while the one in Figure 5.3(a) is still bound to the surface. It is also clear that the one with larger contact angle has traveled further. The same pattern is seen in Figure 5.4, where the droplet locations after 0.48 milliseconds are presented for the case with a large droplet and high relative velocity. It is clear that the droplet with smaller contact angle, 5.4(a), is stronger bound to the surface and thereby spreading out more than the one with large contact angle which stays together keeping the shape of a droplet.

From those simulations, it can be concluded that a higher contact angle results in a faster sliding droplet and thereby faster separation. It can also be seen that in the case with small contact angle a thin water film is left behind the sliding droplet.

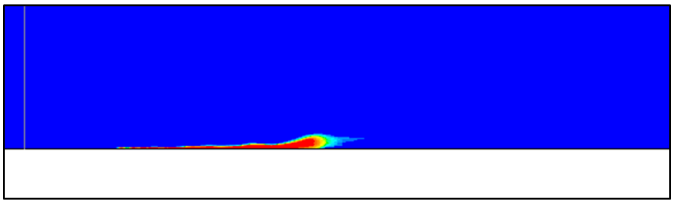

(a) 20° contact angle, 0.5 μl and a normalized relative velocity of 0.42.

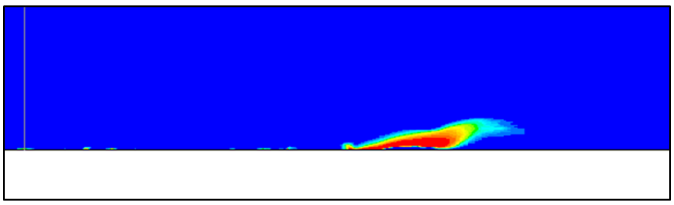

(b) 80° contact angle, 0.5 μl and a normalized relative velocity of 0.42.

Figure 5.3: Droplet position after 1.2 milliseconds. The vertical line on the left in the figures indicates the starting position.

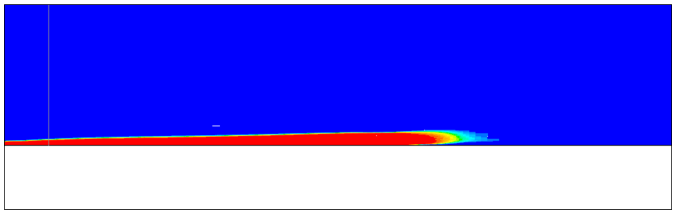

(a) 20° contact angle, 30 μl and a normalized relative velocity of 1.

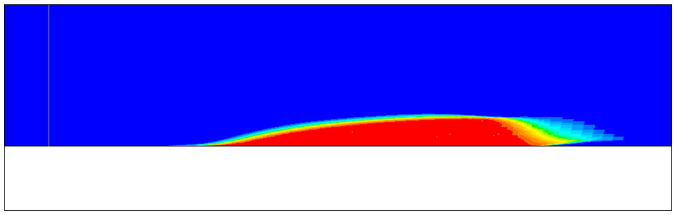

(b) 80° contact angle, 30 μl and a normalized relative velocity of 1.

Figure 5.4: Droplet position after 0.48 milliseconds. The vertical line on the left in the figures indicates the droplet starting position.

5.3.2 Droplet size

As for the contact angle, there are four pairs of simulations where the only parameter changed is the droplet volume. For investigation of droplet size effects, those pairs are compared one by one.

In Figures 5.5 and 5.6 it is seen that the larger droplet has been sliding a longer distance during the same amount of time, but when investigating the small droplet closely it can be seen that it is detached from the surface. From this it can be concluded that larger droplets are moving faster along the surface but smaller droplet require less time to separate from the surface.

The higher sliding velocity for the large droplet can be due to the fact that the droplet is "higher" and therefore stretching longer out in the boundary layer and thereby is more affected by the air flow.

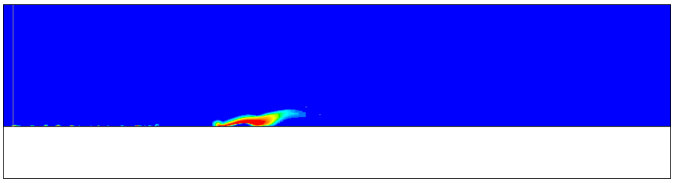

(a) 0.5 μl, 80° contact angle and a normalized relative velocity of 0.42.

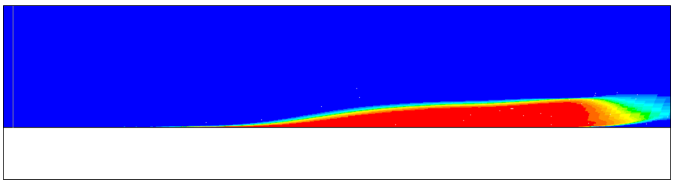

(b) 30 μl, 80° contact angle and a normalized relative velocity of 0.42.

Figure 5.5: Droplet position after 1.34 milliseconds. The vertical line on the very left indicates the droplet starting position.

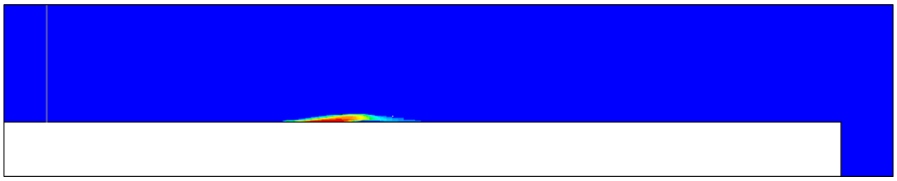

(a) 0.5 μl, 80° contact angle and a normalized relative velocity of 1.

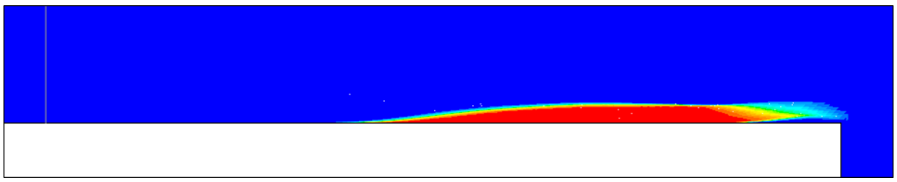

(b) 30 μl, 80° contact angle and a normalized relative velocity of 1.

Figure 5.6: Droplet position after 0.87 milliseconds. The vertical line on the very left indicates the droplet starting position.

5.3.3 Velocity

The gas flow velocity effects is, as for the previous parameters, evaluated by comparing the simulations two and two.

Looking at Figure 5.7 confirms the intuitive guesses that a higher gas flow velocity force the droplet to move faster. The sliding behavior is the same for both flow velocities, the only difference is that everything goes faster in the case with high velocity. The detachment process is faster with a high relative velocity between the dispersed and the continuous phase.

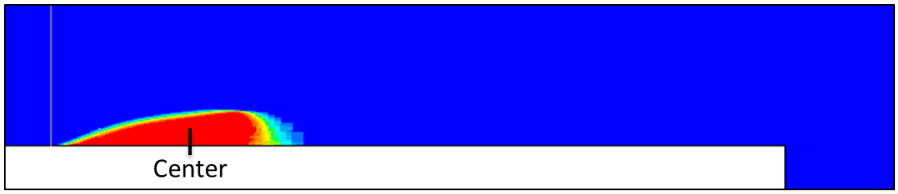

(a) A normalized relative velocity of 0.42, 30 μl and 80° contact angle.

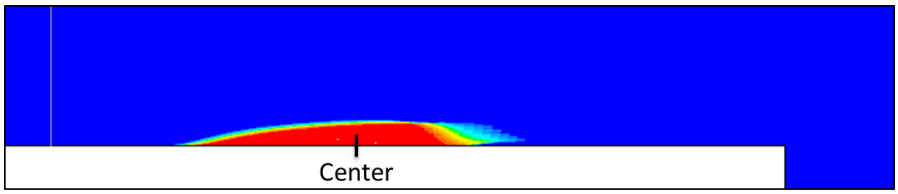

(b) A normalized relative velocity of 1, 30 μl and 80° contact angle.

Figure 5.7: Droplet position after 0.48 milliseconds. Also the center of gravity is indicated to show how far the droplet has been sliding. The vertical line to the left indicates the starting position of the droplet.

5.4 Centrifugal force

The centrifugal acceleration of the woodchips was calculated by dividing Equation (2.9) by the mass m. Inserting a normalized velocity of 0.33 and a normalized radius of 1 gave a centrifugal acceleration some hundred times the gravitational acceleration. Including the centrifugal acceleration, as described in section 3.1.9, the separation process was more accurately described and it was possible to estimate how the detachment will take place from differently orientated woodchips. In those simulations a droplet volume of 15 μl, a contact angle of 40° and a normalized relative flow velocity of 0.75 was used. The simulations were made with a single droplet placed on the woodchip center.

In Figures 5.8 the position of the droplets after 1 millisecond are displayed for the different cases. It can be seen that the more the force is directed upwards, the faster the droplet detaches from the surface. In the cases with a downwardly directed force, the droplet keeps sliding on the surface instead. Even in those cases, with a downwardly directed force, the droplets are sliding fast on the surface thanks to the shearing air flow. From those simulations it can be concluded that the droplets will separate from the surface in a time frame of just over two milliseconds.

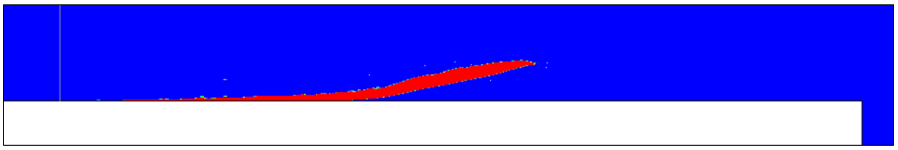

(a) Centrifugal acceleration directed upward.

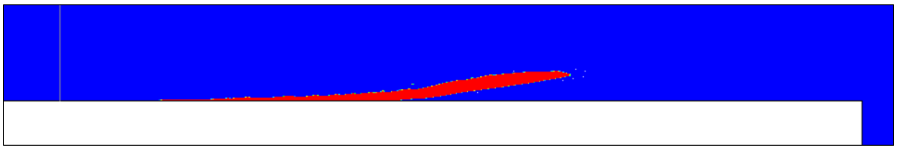

(b) Centrifugal acceleration directed upward and to the right.

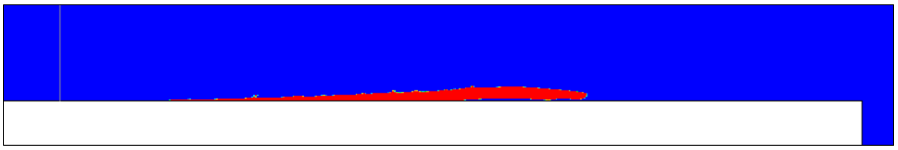

(c) Centrifugal acceleration directed to the right.

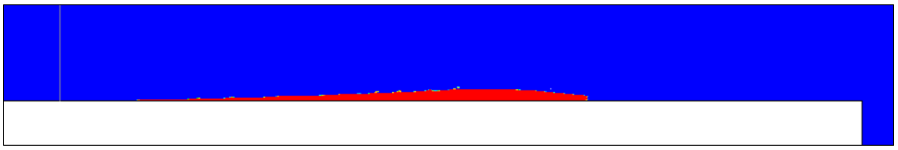

(d) Centrifugal acceleration directed downward and to the right.

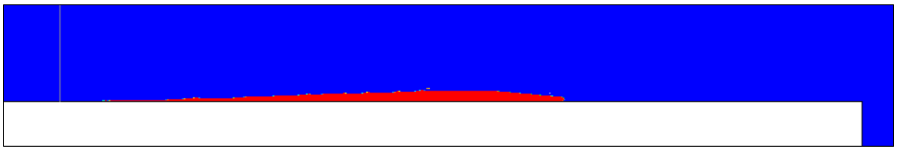

(e) Centrifugal acceleration directed downward.

Figure 5.8: Droplet position after 1 millisecond. The vertical line on the left shows the droplet's starting point, i.e. the woodchip center.

5.5 Film on surface

For a liquid film flowing down an inclined surface with gravity as the driving mechanism the flow velocity can be calculated by hand. The derivation of the formulas is carried out in Appendix C, resulting in the following equations for the flow profile and the average velocity:

$$u_x(y) = \frac{\rho g sin\theta}{2\mu} y\,(2h - y) \tag{5.1}$$

$$u_{avg} = \frac{2}{3}\frac{\rho g h^2 sin\theta}{2\mu} = \frac{2}{3} u_{max} \tag{5.2}$$

Consider a single woodchip covered with a water film with a thickness of 1 mm and the

centrifugal force directed as in Figure 3.4(e). With gravitational acceleration only, the average velocity of the water film would be 4.9 m/s resulting in that it takes about 12 milliseconds for the water film to run off a 6 cm long woodchip. With the centrifugal acceleration calculated in section 5.4 as the driving force, the average velocity is some hundred times higher and the time for the film to run off the woodchip is much shorter. In those calculations no attractive forces between the surface and the water film are included, therefore the time will be significantly increased in reality.

5.6 3D

The three dimensional simulation turned out to be very computationally heavy and time consuming. To fit within the time frame of this thesis only a short period of time was simulated. The positions of the droplets after 0.17 milliseconds are shown in Figure 5.9. It can be seen that the droplets are deformed and start to slide in the same way as the droplets did in the two dimensional simulations presented above.

Figure 5.9: Droplet positions after 0.17 milliseconds seen from the side.

6 Conclusions and discussion

From the theory, it was expected that a large contact angle would be beneficial for the phase separation and this was also shown by the simulations. From this it is concluded that the time between press and cyclone is one of the most important parameters and should be as low as possible. It is a matter of seconds. Based on Figure 2.6(b), one could argue that the use of old woodchips would be beneficial because they have a much larger constant wetting rate angle than fresh chips have. But this would in turn result in that the moisture that was pressed out in the press will be reabsorbed. If no surface water is present when the chips are loaded into the cyclone, the detachment process is not possible. Therefore, if using old woodchips, they must be pressed again, which will generate in creation of new surfaces with a low constant wetting rate angle. Based on this, it is concluded that the time between press and cyclone must be just very few seconds, independently of the age of the woodchips.

Regarding the transport of woodchips from the press to the cyclone, it was shortly mentioned in the chapter about the experiments, that one possibility is to use a conveyor belt with some kind of vacuum suction in order to remove excess moisture before the cyclone. But in that case a second press should be used just before the cyclone, to press out more water, including the water that have been reabsorbed since the first press, and to get as large contact angles as possible. The cyclone inlet should, if possible, be placed just under the press outlet. Another way to increase the drying rate might be to have a system of two press-and-cyclone units in series. This might be beneficial since the experiments showed that the first percentages were the cheapest to separate.

From the simulations it was seen that the phase separation was easier with smaller droplets. One way to reduce the droplet size might be to remove more moisture before the (last) cyclone, since less water would most likely result in smaller droplets. As mentioned, a conveyor belt with suction might be used to reduce the amount of water sent into cyclone, a thereby this might decrease the time for droplet detachment. Also the series connection mentioned above might be beneficial since this would reduce the amount of water that goes into the last cyclone.

Considering the effects of relative velocity, it was shown that higher relative velocity accelerates the detachment process. This tells that the blower speed should be high. For smaller particles, the Stokes number will be reduced, i.e. they will follow the flow to a much greater extent than larger particles. Therefore, the woodchips should not be too small because this will result in a reduced relative velocity.

The cyclone is originally a separation unit and can, as said, be used for classification of particles by their size. In the experiments, this was seen in the way that the smallest particles were following the gaseous phase through the gas outlet over head. Those particles were found all dry, but they might, to a large extent, have been dried by evaporation.

Regarding the size and design of the press-cyclone unit it can be said that it is mobile, and therefore rather easy to transport to the tree felling site. In that way the transport distance for

logs can be reduced. The cyclone itself is not containing any moving parts and in combination with that it is operating at atmospheric pressure this will minimize the maintenance. It must also be said that the air flow is not preheated, therefore no thermal drying, even though some evaporation will occur due to lower partial pressure of water in the air phase than the vapor pressure of water.

From the experiments it was concluded that the feed rate was the parameter with highest effect on the responses. Depending on the specifications for the product, there will be a trade off if it is desired to remove a large amount of moisture per time unit, achieved with a high feed rate, or to get as dry product as possible, favored by low feed rate. A high feed rate results in shorter residence time and thereby the processing time is reduced and the production is increased.

Concerning the simulations and the dynamic mesh adaption, it might have been more computationally effective to initially refine the mesh much enough in the area where the droplet will move since it is computationally expensive to change the mesh during the solution procedure. This was not investigated further in this thesis but it should be kept in mind.

The droplets in the trend study, see Figures 5.3 to 5.7, take a light blue color at the front end. This indicates a mixture of water and air in those cells, which is not really the physical reality. To get the right physics, the interface should be represented over just a few cells, as in Figure 5.8 where no "transition-zone" is seen. The difference is due to the volume-fraction discretization scheme and the droplet resolution. Even though this transition-zone is present in the trend study simulations, the trends are still to be considered valid and evaluable. The traveled distance and separation was confirmed with the same settings and resolution as in the simulations with different centrifugal acceleration.

Worth to mention is also that when performing VOF simulations in two dimensions, the surface tension will, off course, only act in two dimensions, therefore the droplets will stretch and finally get the serpentine shape as is seen in Figure 5.8, which will not be the case in reality. Working with a 3D case instead, the surface tension will keep the droplet more "drop-like" but as indicated before, the time frame of this thesis left that for future work.

It must also be noted that there are other effects that have been neglected in this thesis, that in the real case would assist the separation. For example woodchips rotating around their own axis and collisions with the cyclone walls would probably assist the detachment process.

7 Future work

This thesis is part of a larger project and represents a first study of the detachment process separating liquid droplets from solid surfaces and will thereby act as a base for future work.

The simulations in this thesis focus only on the droplet sliding and detachment and do not include the evaporation of water. For future work it would be a logic step to include also evaporation in order to examine how much of the moisture is evaporated and how much is separated due to phase separation. In combination with this, experimental measurements of the humidity inside to cyclone should be conducted.

The actual behavior of the woodchips inside the cyclone must be closely investigated by experiments in order to estimate how the woodchips are interacting and if there are collisions with the cyclone walls, which would have effects on the process. It would also be interesting to perform simulations of woodchips entirely covered with a water film.

Bibliography

[1] United Nations, "Global Issues: Climate Change". [Online]. Available: http://www.un.org/en/globalissues/climatechange. [Accessed: October 2013].

[2] European Commision, "The EU climate and energy package". [Online]. Available: http://ec.europa.eu/clima/policies/package/index_en.htm. [Accessed: October 2013].

[3] Eurostat, "Share of renewable energy in gross final energy consumption", European Commission Eurostat. [Online]. Available: http://epp.eurostat.ec.europa.eu/tgm/table.do?tab=table&init=1&language=en&pcode=tsdcc110&plugin=1. [Accessed: December 2013].

[4] Forest Products Laboratory, *Wood Handbook - Wood as an Engineering Material*, U.S. Department of Agriculture, 2001. [E-book]. Available: Knovel. http://app.knovel.com/hotlink/toc/id:kpWHWEM00F/wood-handbook-wood-an.

[5] M. Vert, Y. Doi, K.-H. Hellwich, M. Hess, P. Hodge, P. Kubisa, M. Rinaudo and F. Schué, "Terminology for biorelated polymers and applications (IUPAC Recommendations 2012)", *Pure and Applied Chemistry*, vol. 84, no. 2, pp. 377-410, 2012.

[6] U.S. Geological Survey, science for a changing world, National Water-Quality Assessment Program, "Glossary". [Online]. Available: http://water.usgs.gov/nawqa/glos.html. [Accessed: November 2013].

[7] P. I. Morris and J. E. Winandy, "Limiting Conditions for Decay in Wood Systems", *The International Research Group on Wood Preservation*, Paper prepared for the 33rd Annual Meeting, 2002.

[8] B. M. Jenkins, L. L. Baxter, T. R. Miles Jr. and T. R. Miles, "Combustion properties of biomass", *Fuel Processing Technology*, vol. 54, pp. 17-46, 1998.

[9] J. Nurmi, "Heating Values of Mature Trees", *Acta Forestalia Fennica*, vol. 256, 1997.

[10] J. D. Seader and E. J. Henley, *Separation Process Principles*, second edition. Hoboken, NJ: John Wiley & Sons, Inc., 2006.

[11] SMHI, "Luftfuktighet", Sveriges meterologiska och hydrologiska institut. [Online]. Available: http://www.smhi.se/kunskapsbanken/meteorologi/luftfuktighet-1.3910. [Accessed: November 2013].

[12] P. Atkins and L. Jones, *Chemical Principles: The Quest for Insight*, fourth edition. New York: W. H. Freeman, 2008.

[13] The Engineering ToolBox, "Water Saturation Pressure". [Online]. Available: http://www.engineeringtoolbox.com/water-vapor-saturation-pressure-d_599.html. [Accessed: January 2014].

[14] V. Belessiotis and E. Delyannis, "Solar Drying", *Solar Energy*, vol. 85, pp. 1665-1691, 2011.

[15] P.-G. de Gennes, F. Brochard-Wyart and D. Quéré, *Capillarity and Wetting Phenomena: Drops, Bubbles, Pearls, Waves*. New York: Springer Science+Business Media, 2004.

[16] J. Welty, C. Wicks, R. Wilson and G. Rorrer, *Fundamentals of Momentum, Heat and Mass Transfer*, fifth edition. Hoboken, NJ: John Wiley & Sons, Inc., 2008.

[17] R. M. Nussbaum, "Natural surface inactivation of Scots pine and Norway spruce evaluated by contact angle measurements", *Holz als Roh- und Werkstoff*, vol. 57, no. 6, pp. 419-424, 1999.

[18] L. Gao and T. J. McCarthy, "Contact Angle Hysteresis Explained", *Langmuir: the ACS journal of surfaces and colloids*, vol. 22, no. 14, pp. 6234-6237, 2006.

[19] P. G. de Gennes, "Wetting: statics and dynamics", *Reviews of Modern Physics*, vol. 57, no. 3, pp. 827-863, 1985.

[20] C. W. Extrand and Y. Kumagai, "Liquid Drops on an Inclined Plane: The Relation between Contact Angles, Drop Shape, and Retentive Force", *Journal of Colloid and Interface Science*, vol. 170, no. 2, pp. 515-521, 1995.

[21] E. Pierce, F. J. Carmona and A. Amirfazli, "Understanding of sliding and contact angle results in tilted plate experiments", *Colloids and Surfaces A: Physicochemical and Engineering Aspects*, vol. 323, no. 1, pp. 73 - 82, 2008.

[22] C. Antonini, F. J. Carmona, E. Pierce, M. Marengo and A. Amirfazli, "General Methodology for Evaluating the Adhesion Force of Drops and Bubbles on Solid Surfaces", *Langmuir: the ACS journal of surfaces and colloids*, vol. 25, no. 11, pp. 6143-6154, 2009.

[23] A. J. Hoekstra, *Gas Flow Field and Collection Efficiency of Cyclone Separators*, [Dissertation], Delft University of Technology, Delft, 2000.

[24] A. C. Hoffmann and L. E. Stein, *Gas Cyclones and Swirl Tubes: Principles, Design and Operation*, second edition. New York: Springer-Verlag Berlin Heidelberg, 2008.

[25] H. K. Versteeg and W Malalasekera, *An Introduction to Computational Fluid Dynamics: The Finite Volume Method*, second edition. Glasgow: Pearson Education Limited, 2007.

[26] ANSYS Inc., *ANSYS FLUENT Theory Guide*, release 14.5, 2012.

[27] B. Andersson, R. Andersson, L. Håkansson, M. Mortensen, R. Sudiyo and B. van Wachem, *Computational Fluid Dynamics for Engineers*, ninth edition: internal Chalmeres version. Gothenburg: Cambridge University Press, 2013.

[28] ANSYS Inc., *ANSYS FLUENT Users Guide*, release 14.5, 2012.

[29] J. S. Marshall and W. McK. Palmer, "The distribution of raindrops with size", *Journal of Meteorology*, vol. 5, no. 4, pp. 165-166, 1948.

[30] Internal report at ALTEN Sverige AB, 2013.

[31] Internal report at ALTEN Sverige AB, 2013.

A Droplet calculations

A droplet deposited on a solid surface will take the shape of a spherical cap, as illustrated by the blue part of Figure A.1.

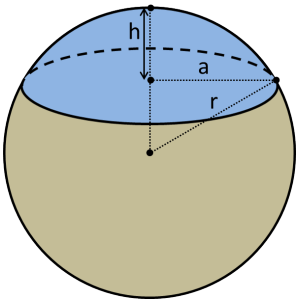

Figure A.1: The spherical cap, shown in blue, is characterized by it's base a and height h and is part of a sphere with radius r.

The volume of a spherical cap is calculated by Equation (A.1), where a and h are defined by Equations (A.2) and shown in Figure A.1.

$$V = \frac{\pi h}{6}(3a^2 + h^2) \tag{A.1}$$

$$a = r \cdot cos(90 - \theta_E) \tag{A.2a}$$

$$h = r(1 - sin(90 - \theta_E)) \tag{A.2b}$$

Inserting (A.2a) and (A.2b) in (A.1) gives:

$$V = r^3 \frac{\pi}{6} \left[1 - sin(90 - \theta_E)\right] \left[3cos^2(90 - \theta_E) + (1 - sin(90 - \theta_E))^2\right] \tag{A.3}$$

Solving (A.3) for r, with desired volume and contact angle, θ_E, and thereafter inserting into the equations for a and h gives the values to use when patching the droplets in the simulations.

Table A.1: Measurements of used droplets.

θ_E [°]	V [μl]	r [mm]	a [mm]	h [mm]
20	0.5	3.54	1.21	0.214
20	30	13.9	4.75	0.838
80	0.5	0.685	0.675	0.566
80	30	2.68	2.64	2.22
40	15	4.56	2.93	1.07

B Forces on dispersed particles

Performing full scale simulations of a cyclone with woodchips, they are modeled with discrete particle modeling, dpm. With this method the particles must be smaller than the computational cells and the forces that might be encountered for are described below. Since the particles are smaller than the computational cells the absolute details around each and every particle are not resolved. If it is desired to include the effects of the particulate phase on the dispersed phase, this is done by inclusion of a source term.

For a single particle, the equation of motion can be written as Equation (B.1), where p denotes the particulate phase and i is particle i. The right hand side is a summation of all forces acting on the particle and they are described in more detail below.

$$m_p \frac{dU_{i,p}}{dt} = \sum F_i \tag{B.1}$$

Drag force
The drag force is written as Equation (B.2) and is due to the relative velocity between the particle and the fluid. A_p is the particle area projected in the direction of the flow, C_D is the drag coefficient, which is a scalar for spherical particles. For non-spherical particles, much more complex formulations are required. Note that Equation (B.2) is valid only for systems with a low particle loading and that adjustments are available for high loading systems.

$$F_{drag} = \frac{1}{2} A_p C_D \rho_f |U_f - U_p| (U_f - U_p) \tag{B.2}$$

Pressure and shear force
Any pressure and shear gradients over the particle surface give rise to pressure and shear forces which can be stated as Equation (B.3), where V_p is the particle volume.

$$F_{press} = V_p \left(-\frac{\partial P}{\partial x_i} + \frac{\partial \tau_{ij}}{\partial x_j} \right) \tag{B.3}$$

Very small particles and a uniform pressure distribution in the system should result in small gradients over the particle surface and in that case this force can be neglected.

Added Mass force
When there is a relative acceleration between the particle and the fluid, this will result in that the fluid closest to the particle is accelerated with the particle and thereby the particle appears heavier than it actually is. This force can be expressed as Equation (B.4).

$$F_{added\,mass} = -C_{VM} \rho_f V_p \frac{D}{Dt} (U_p - U_f) \tag{B.4}$$

This force is an effect of the relative acceleration between the phases, therefore it can be neglected when the relative acceleration is low and also when the density ratio ρ_f / ρ_p is very low.

History force
The history force, also called the Basset force, is due to a delay in the boundary layer development, for example in very viscous fluids. The derivation of this force is very time consuming and since it is usually small in comparison to it's effects it is usually neglected. It is square dependent on the particle diameter and can therefore be neglected for small particles, as for low viscosity fluids.

Buoyancy and gravity force
The buoyancy force is a lift force acting on the particle by the fluid. It arises from the fluid that is displaced by the particle, refer to Archimedes' principle that states that the buoyancy force is equal to the weight of the fluid displaced by the object. The gravity force is due to the gravitational field surrounding Earth.

$$F_{buoy+grav} = V_p\, g(\rho_f - \rho_p) \tag{B.5}$$

For very small particles and in cases with low fluid density, the buoyancy contribution in the above equation can be neglected.

Magnus force
For rotating particles, the relative velocity between fluid and particle will be different on the different sides of the particle. This will give rise to a pressure difference and thereby a lift force called the Magnus force is directed towards the side with lower relative velocity. Since the Magnus lift force is not well defined outside the laminar region and in combination with that it is usually small, it is not discussed further. Can be neglected for small particles.

Saffman lift force
As the Magnus force, the Saffman force is due to a pressure difference between the sides of the particle. The Saffman lift force arises when the particle is flowing in a velocity gradient, e.g. in a boundary layer. Can be neglected for small particles and low fluid viscosity.

Thermophoretic force
Warm molecules are moving faster than cold ones and in flows with a temperature gradient this fact will give rise to the thermophoretic force acting in the direction towards the coldest side. The thermophoretic force is only important for small particles and will thereby cause a separation of particles by size. Can usually be neglected because only important for very small particles.

Brownian motion
The Brownian motion will add a random parameter to the particle motion because of random collisions between particles and fluid molecules. The Brownian motion is relevant only for particles on submicrometer scale [27]. In Fluent, the Brownian motion is only to be included in laminar flows, for turbulent cases the effects are encountered for by the turbulent force [26].

Turbulent force
To account for turbulent irregularities, a random addition is added to the fluid velocity. The time of implementation is taken as the smallest of the lifetime of a turbulent eddy and the time it takes for a particle to move through a turbulent eddy.

C Film flow down an inclined surface

The overall balance of linear momentum for a control volume is expressed by the momentum theorem written in Equation (C.1), where **F** is the forces acting on the fluid.

$$\sum \mathbf{F} = \int \int_{c.s.} \rho \mathbf{u} (\mathbf{u} \cdot \mathbf{n}) \, dA + \frac{\partial}{\partial t} \int \int \int_{c.v.} \rho \mathbf{u} \, dV \tag{C.1}$$

In Figure C.1 the two dimensional flow of a liquid film down an inclined surface is displayed. The film thickness is h and the flow is driven by gravity.

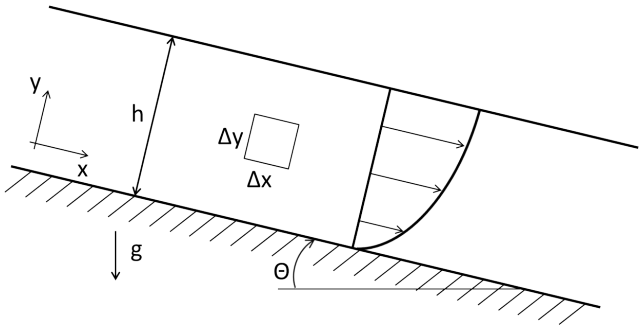

Figure C.1: Gravity driven film flow down the surface of an inclined plane.

Evaluation of Equation (C.1) in x-direction, for the above case, gives:

$$\sum F_x = \int \int_{c.s.} \rho u_x (\mathbf{u} \cdot \mathbf{n}) \, dA + \frac{\partial}{\partial t} \int \int \int_{c.v.} \rho u_x \, dV \tag{C.2}$$

Separate evaluation of the terms in Equation (C.2) for the fluid element displayed in Figure C.1 gives:

$$\sum F_x = P\Delta y|_x - P\Delta y|_{x+\Delta x} + \tau_{yx}\Delta x|_{y+\Delta y} - \tau_{yx}\Delta x|_y + \rho g sin\theta \Delta x \Delta y \Delta z \tag{C.3a}$$

$$\int \int_{c.s.} \rho u_x (\mathbf{u} \cdot \mathbf{n}) \, dA = \rho u_x^2 \Delta y|_{x+\Delta x} - \rho u_x^2 \Delta y|_x \tag{C.3b}$$

$$\frac{\partial}{\partial t} \int \int \int_{c.v.} \rho u_x \, dV = 0 \tag{C.3c}$$

With a free liquid surface, the pressure terms eliminate, and for a fully developed flow the convective momentum terms cancel out, thereby (C.3b) is zero. Equation (C.2) simplifies to:

$$\tau_{yx}\Delta x|_{y+\Delta y} - \tau_{yx}\Delta x|_{y} + \rho g sin\theta \Delta x \Delta y = 0 \tag{C.4}$$

Dividing by the control element volume, $\Delta x \Delta y(1)$, and in the limit $\Delta y \to 0$, the following differential equation results:

$$\frac{d}{dy}\tau_{yx} + \rho g sin\theta = 0 \tag{C.5}$$

The no slip boundary condition at the wall requires the velocity to vanish at y=0 and the free surface condition at y=h requires that the shear stress is equal to zero here. Integrating Equation (C.5), inserting the boundary conditions just mentioned and using $\tau_{yx} = \mu(du_x/dy)$ gives the following velocity profile:

$$u_x(y) = \frac{\rho g sin\theta}{2\mu} y\,(2h - y) \tag{C.6}$$

The average velocity is calculated below.

$$\begin{aligned} u_{avg} &= \frac{1}{A}\int\int_A u\,dA \\ &= \frac{1}{\Delta y \Delta z}\int\int_A \frac{\rho g sin\theta}{2\mu} y\,(2h - y)\,dy\,dz \\ &= \frac{1}{h\Delta z}\int_0^{\Delta z}\int_0^h \frac{\rho g sin\theta}{2\mu}(2hy - y^2)\,dy\,dz \\ &= \frac{\rho g sin\theta}{2\mu h}\left[hy^2 - \frac{y^3}{3}\right]_0^h \\ &= \frac{\rho g sin\theta}{2\mu}\left[h^2 - \frac{h^2}{3}\right] \\ &= \frac{2}{3}\frac{\rho g h^2 sin\theta}{2\mu} = \frac{2}{3}u_{max} \end{aligned} \tag{C.7}$$

D Pressure

Figure D.1 shows a contour plot of the pressure profile around the sliding droplet. It was investigated if the flow resulted in a slightly lower pressure just above the droplet surface, which would thereby facilitate the detachment process, but no such profile was seen.

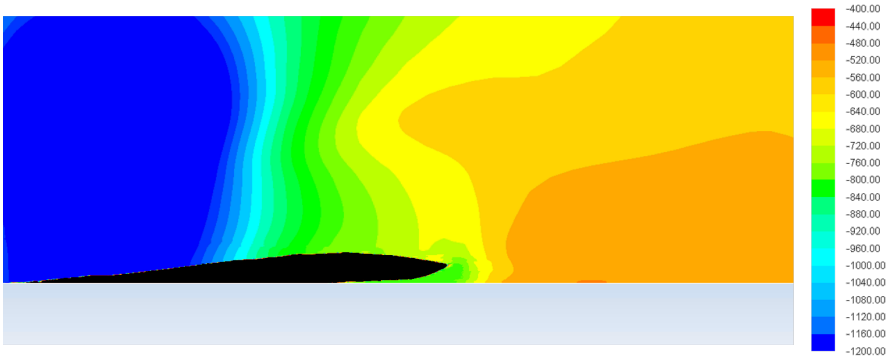

Figure D.1: The pressure profile around a droplet on the woodchip surface. The droplet is colored in black.

E Turbulent viscosity

To evaluate whether the model can handle damping of the turbulent viscosity at the droplet surface, Figure E.1 shows a contour plot of the turbulent viscosity around the sliding droplet. The liquid surface of the droplet should damp the turbulence in the same way as a solid surface does and from Figure E.1 it can be seen that the model handles this in a good way.

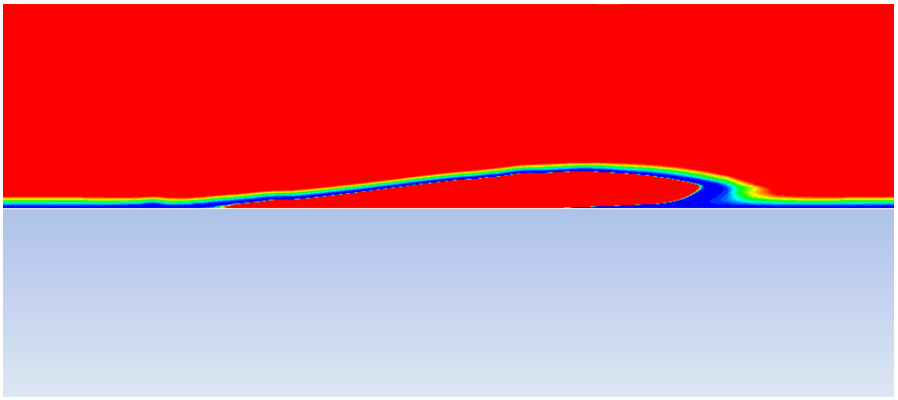

Figure E.1: Turbulent viscosity.